ANODE CATALYST LAYER ENGINEERING FOR THE DIRECT FORMIC ACID FUEL
CELL

by

Sanam Sanii

B.A.Sc., University of British Columbia, 2008

A THESIS SUBMITTED IN PARTIAL FULFILLMENT OF
THE REQUIREMENTS FOR THE DEGREE OF

MASTER OF APPLIED SCIENCE

in

THE FACULTY OF GRADUATE STUDIES

(Chemical and Biological Engineering)

THE UNIVERSITY OF BRITISH COLUMBIA
(Vancouver)

February 2011

Abstract

        Direct formic acid fuel cells (DFAFC) are promising alternatives to hydrogen proton exchange membrane fuel cells for microelectronic applications. Compared to direct methanol fuel cell (DMFC), the main advantages of direct formic acid fuel cell (DFAFC) are higher theoretical open circuit voltage (1.45 V at 298 K), lower fuel cross over towards cathode and reasonable power densities at room temperature that make DFAFCs a viable alternative for micropower applications. The operation of DFAFCs on Pd-based catalysts at ambient temperature showed lower fuel permeation from anode to cathode that resulted in better fuel utilization when running on high formic acid concentrations (~10M). However, Pd suffers an unacceptable loss of performance with time that decreases the cell power density by about 50% in a few hours.

        The aim of the present work is to create an extended reaction zone anode structure to improve the utilization of the catalyst and to modify the electrode surface characteristics in order to reduce performance losses. The novel catalyst deposition technique involved electroless (chemical) deposition of Pd particles directly onto the carbon paper substrate (AvCarbTM P50) in the presence of Nafion® solution. It was found that the use of 4.66 g L^{-1} of pure Nafion® as an additive to the electroless bath and Shipley pre-treatment resulted in 1.6 mg cm^{-2} and 0.07 mg cm^{-2} Pd and Sn mass loadings respectively with Pd average particle size of 0.45 to 0.55 μm. When pre-treating in nitric acid solution, the surface coverage was found to be uniform with dense particulate-like structure.

        The surface nitric acid pre-treatment method in conjunction with 2.46 g L^{-1} Nafion® additive in the electroless solution were resulted in 4.5 mg cm^{-2} Pd mass loading on AvCarbTM P50 and enhanced electrochemical performance at current densities larger than 500 A m^{-2} at 333 K . Comparing the Pd/C and PdSn/C performances in DFAFC tests, the Pd/C anode with higher Pd mass loading (4.5 mg cm^{-2}) and OCV stayed fairly stable on ~ 0.55 V up to 3.5 hours of constant current draw(100 A m^{-2} at 333 K).

Table of contents

List of tables

List of figures

List of symbols

A	**Electrode Area**	m^2
a_i	**Chemical Activity**	-
C	**Concentration**	Molarity or mol m^{-3}
b	**Tafel Slope**	V decade^{-1}
C_o	**Initial Concentration**	mol m^{-3}
c_b	**Bulk Concentration**	mol m^{-3}
c_s	**Surface Concentration**	mol m^{-3}
d	**Electrode Spacing**	m
D	**Diffusion Coefficient**	$m^2\,s^{-1}$
E	**Cell Voltage**	V
E_e	**Equilibrium Cell Potential**	V
$E_{e,anode}$	**Anode Equilibrium Cell Potential**	V
$E_{e,cathode}$	**Cathode Equilibrium Cell Potential**	V
E_{actual}	**Actual Cell Potential**	V
E^o	**Standard Cell Potential (T= 298 K)**	V
F	**Faraday's Constant**	96485 C mol^{-1}
i	**Current Density per Geometric Area**	A m^{-2}
i_o	**Exchange Current Density**	A m^{-2}
i_p	**Peak Current Density**	A
i_L	**Limiting Current Density**	A m^{-2}
k_m	**Mass Transport Coefficient**	m s^{-1}
κ	**Electrolyte Conductivity**	S m^{-1}
M_i	**Electrochemical Species**	-
n	**Number of Electrons Transferred/molecule**	-
n^*	**Number of Electrons Transferred in Rate Determining Step**	-
P	**Pressure**	atm or bar
P^*	**Power Density**	W m^{-2}
q	**Heat**	J
R	**Gas Constant**	8.31 J K^{-1} mol^{-1}
S_i	**Reactant Stoichiometric Coefficient**	-
T	**Temperature**	K
t	**Time**	Sec
t_o	**Initial Time**	Sec

V	**Volume**	m^3
W	**Work**	J
W$_e$	**Electric Work**	J
α	**Transfer Coefficient**	-
α*	**Charge Transfer Coefficient**	-
α$_a$	**Anodic Charge Transfer Coefficient**	-
δ	**Diffusion Layer Thickness**	m
α$_c$	**Cathodic Charge Transfer Coefficient**	-
ν_s	**Scan Rate**	$V\ s^{-1}$
ΔG	**Change in Gibbs Free Energy**	$J\ mol^{-1}$
ΔGo	**Standard System Gibbs Free Energy (T= 273K , P=1 atm)**	$J\ mol^{-1}$
ΔH	**Change in Enthalpy**	$J\ mol^{-1}$
ΔS	**Change in Entropy**	$J\ mol^{-1}\ K^{-1}$
ΔU	**Change in Internal Energy**	$J\ mol^{-1}$
ΔV	**Change in Potential (Potential Difference)**	V
Δφ$_{ohm}$	**Ohmic Losses**	V
Δφ$_{ionic}$	**Ionic Losses (Resistance)**	V
Κ	**Conductivity**	$S\ m^{-1}$
η	**Over potential**	V
η$_s$	**Surface Over Potential**	V
η$_c$	**Concentration Over potential**	V
η$_{s,anode}$	**Anode Surface Over potential**	V
η$_{s,cathode}$	**Cathode Surface Over potential**	V
η$_{c,anode}$	**Anode Concentration Over potential**	V
η$_{c,cathode}$	**Cathode Concentration Over potential**	V

List of abbreviations

AFC	**Alkaline Fuel Cell**
BEC	**Butler-Volmer-Erdey- Cruz**
CA	**Chronoamperometry**
CCM	**Catalyst Coated Membrane**
CP	**Chronopoteniometry**
CV	**Cyclic Voltammetry**
DFAFC	**Direct Formic Acid Fuel Cell**
DMFC	**Direct Methanol Fuel Cell**
GDE	**Gas-Diffusion Electrode**
GF	**Graphite Felt**
ICP-AES	**Inductively Coupled Plasma Atomic Emission Spectroscopy**
IUPAC	**International Union of Pure and Applied Chemistry**
MEA	**Membrane-Electrode Assembly**
MSE	**Mercury-Mercurous Sulphate Reference Electrode**
OCV	**Open-Circuit Voltage**
PEMFC	**Proton Exchange Membrane Fuel Cell**
SEM	**Scanning Electron Microscope**
SHE	**Standard Hydrogen Electrode**
STP	**Standard Temperature and Pressure**

Acknowledgements

1.0   Introduction

It is estimated about 85% of the developed world's energy was supplied by fossil fuels-largely petroleum, natural gas, and coal as 2002 (Tester, Drake, & Golay, 2005). It is well known that, the supplies of these fuels are physically limited and their use threatens our environment. Aside of the global warming issue, burning fossil fuel and release of subsequent chemicals and toxics is problematic to human health and the environment. Nowadays although the world relies heavily on fossil fuels, it is well known that there will be a day when fossil fuels are depleted. Therefore, today more than ever, a sustainable energy supply for the next generation is needed (Ristinen & Kraushaar, 2006). In order to reach a sustainable future in terms of energy use, it is essential to develop a new set of energy technologies to be efficient in production and consumption. Perhaps, a new generation of renewable energy technologies and nuclear options that becomes accepted by the public.

Among many ideas and technology options under research today, electrochemical power sources such as batteries and fuel cell systems that generate electricity are good candidates to be considered. Through use of fuel cells and batteries, we are able to directly generate electricity with no other intermediate energy conversion (Carrette & Friedrich, 2000). In fact, fuel cells now are in great interest as clean energy converters for use in producing electricity for consumers and as the energy source for electric vehicles and portable devices. This interest is motivated by the potential for high fuel-to-electricity conversion efficiencies and by the fact that fuel cells fed with hydrogen emit only water (Ristinen & Kraushaar, 2006).

A fuel cell is an electrochemical system that continuously converts chemical energy of fuel into electrical energy and heat with high thermodynamic efficiency (e.g. efficiency of 80% for H_2/O_2 systems at ambient pressure and temperature) (Miley, Luo, & Mather, 2007). Fuel cells will continue to generate electricity as long as they are fed with both fuel and oxidant. Most common fuel types to be used by fuel cells are pure hydrogen, hydrocarbons, alcohols, and hydrazine with oxygen/air as oxidants (Barbir, 2005).

 In early 1800, William Grove discovered a fuel cell device called "gaseous voltaic battery" which comprised of Pt electrodes and sulphuric acid electrolyte with hydrogen and oxygen as reactants. The basic operating principle of Grove's fuel cell device remains the same

today. In general a fuel cell mechanical structure consists of two electrodes, which are separated by an electrolyte (Barbir, 2005). The electrochemical reactions occur on the electrodes surface and the ions are transported through the electrolyte medium. Fuel cells are classified based on the type of electrolyte, and temperature range as shown in Table 1-1.

Table 1- 1: Comparison of fuel cell types (Blomen & Mugerwa, 1993)

Fuel Cell Type	Electrolyte	Temperature (^{o}C)	Applications
Alkaline Fuel Cell (AFC)	Aqueous potassium hydroxide	90-100	Space ,Military
Phosphoric Acid Fuel cell (PAFC)	Liquid phosphoric acid	175-200	Transportation, Electric utility
Molten Carbonate Fuel cell (MCFC)	Liquid lithium/sodium/potassium carbonates	600-1000	Electric Utility
Solid Oxide Fuel Cell (SOFC)	Solid zirconium oxide	600-1000	Electric Utility
Polymer Electrolyte Membrane fuel cell (PEMFC)	Solid polymer perfluorosulphonic acid	60-100	Portable power, Transportation

Proton exchange membrane fuel cell (PEMFC) systems have been investigated extensively due to their simplicity in design, lower operating temperature, and potential use in portable electronic devices. In proton exchange membrane fuel cells (PEMFC) the membrane acts as the electrolyte which is squeezed between two conductive electrodes (Barbir, 2005). There exists a layer between the porous electrode and the polymer membrane that contains catalyst particles, typically Pt and Pd supported on carbon based material for micro fuel cells (Venugopalan, 2001).

Electrochemical reactions occur at the interface of electrolyte and electrode (noble metal) surface. Protons travel through the electrolyte (membrane) and electrons pass via the conductive electrodes and the external circuit to the other side of the membrane (Blomen & Mugerwa, 1993).

Oxygen or air is continuously fed at the cathode side and water is produced at the cathode as the product of the electrochemical reaction. In this system, the fuel side is negative and it is

called the anode; whereas, the oxygen side of the cell is positive and it is called the cathode (Figure 1-1).
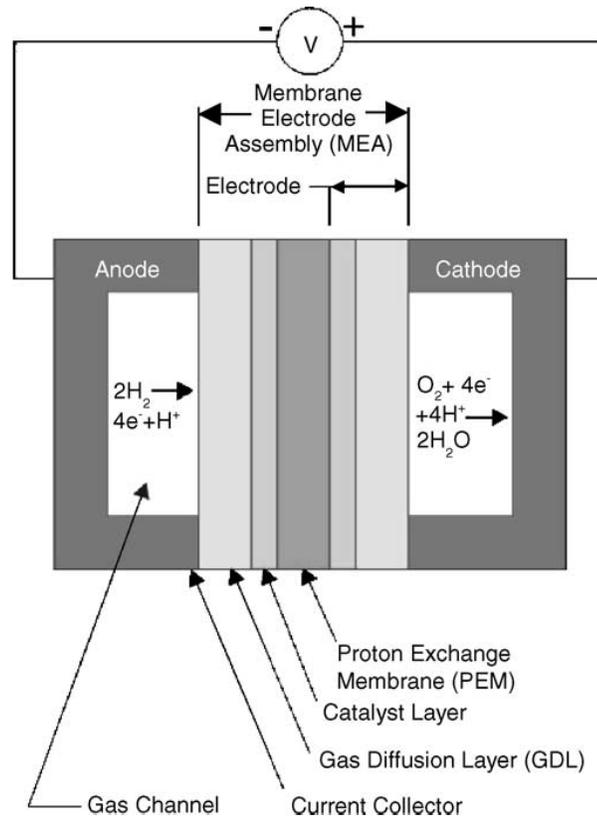
Figure 1-1: Schematic of a proton exchange membrane fuel cell (PEMF) (Lister & McLean, 2004) .

Conventionally, the polymer electrolyte membrane used in PEM fuel cell systems contains sulphonate (-SO$_3$H) groups that facilitate the transport of hydrogen proton (H$^+$) via proton hopping (Grotthuss mechanism) and diffusion (Barbir, 2005). The thin polymer electrolyte membrane of around 50-150 μm reduces the Ohmic resistance that typically exists between the two electrodes and provides a compact design of the system.

Today, the most commonly used electrolyte in PEM fuel cell systems are produced by DuPont Corporation that is a sulfonated tetrafluoroethylene based fluoropolymer-copolymer and was discovered in the late 1960s by Walther Grot of DuPont named as Nafion® (Figure 1-2). It is known that Nafion® is capable of good protonic conductivity, permeability, and

thermal/mechanical stability (Carrette & Friedrich, 2000). For instance the average cost of Nafion® 117 membrane made by Du Pont today is around CAD \$35/100 cm^2 for laboratory use (*http://www.dupont.com*).
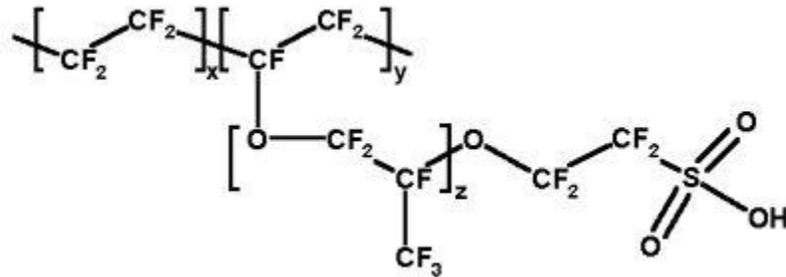
Figure 1-2: Chemical structure of Nafion® (Mauritz & Moore, 2004).

Today, the use of the PEM fuel cells is most commonly demanded by portable electronics (e.g. cellular phone and laptop computers); therefore, PEMFCs potentially could replace batteries in near future. The main advantage of micro fuel cells over batteries is the fact that there is no need to recharge the power source by connecting the system to an electrical grid.

However, one drawback for commercialization of PEM fuel cell is the cost associated with electro catalyst metals such as Pt. Therefore, reconfiguration of the PEM fuel cell is targeted for reducing the amount of Pt-based catalysts in the electrodes. In terms of the fuel option in PEMFC, pure hydrogen is the most studied fuel due to rapid kinetics at the hydrogen fuel cell anode and higher electrical efficiency compared to other fuels (Carrette & Friedrich, 2000).

Nevertheless, hydrogen gas storage, handling, and production are more difficult and dangerous than liquid fuels. Among different liquid fuels, low molecular weight fuels such as formic acid, methanol and ethanol are promising alternative liquid fuels to hydrogen for the PEM fuel cells.

Comparing the theoretical specific energies of methanol and ethanol (6.1 and 8.1 kWh L^1) respectively with gasoline (10-11 kWh L^{-1}) at standard condition, it is seen that both liquid methanol and ethanol have close energies to that of gasoline (Blomen & Mugerwa, 1993).

Methanol has been studied as the fuel source in direct methanol fuel cells (DMFC) for many years. The electrode reactions in DMFC are shown in Equations 1-1 to 1-3.

Anode Reaction:

$$CH_3OH + H_2O \rightarrow CO_2 + 6H^+ + 6e^-$$ $E^o_{298\ K}$= 0.04 V vs. SHE [Eq. 1-1]

Cathode Reaction:

$$1.5\ O_2 + 6H^+ + 6e^- \rightarrow 3H_2O$$ $E^o_{298\ K}$= 1.23 V vs. SHE   [Eq. 1-2]

Net Reaction:

$$CH_3OH + 1.5\ O_2 \rightarrow CO_2 + 2H_2O$$ $E^o_{298\ K}$= 1.19 V vs. SHE   [Eq. 1-3]

However, the DMFC has some disadvantages such as high fuel crossover through the membrane, and low catalyst activity for methanol oxidation at temperatures below 100^oC. As a result, methanol crossover from anode through the electrolyte membrane to cathode side (cathode mixed potential) poisons cathode catalyst and reduces the fuel efficiency (Song & Zhou, 2004). The methanol crossover limits the utilization of high methanol concentrations at generally less than 2 M. In parallel with DMFCs, research is progressing on direct formic acid fuel cells (DFAFCs) as an alternative fuel to methanol in direct fuel cells for portable power applications.

Although formic acid has an energy density (2 kWh L^{-1}) lower than methanol (6.1 kWh L^{-1}), the fuel cell can operate with higher concentration of formic acid solutions due to lower fuel crossover compared to methanol fuel. Consequently, the DFAFCs are quite competitive on an actual fuel energy density basis (based on the maximum fuel concentration).

In addition, the issue of fuel crossover through the membrane is not expected to be a major limitation since formic acid partially dissociates to form formate anions ($HCOO^-$) that are repelled by the sufonic terminal groups in Nafion® membrane resulting in overall lower formic acid crossover. As a result, higher fuel concentrations up to 20 M can be used in DFAFCs compared to DMFCs (Jeonga, Miesse, & Cho, 2007). The most desirable reaction pathway for direct formic acid fuel cells is via the dehydrogenation reaction, which does not form CO as a reaction intermediate. Formic acid reactions in anode and cathode are shown below (Equation 1-4, 1-5 and 1-6).

Anode Reaction:

$$HCOOH \rightarrow CO_2 + 2 H^+ + 2 e^-$$ $E^o_{298 K}= - 0.22$ V vs. SHE   [Eq. 1-4]

Cathode Reaction:

$$1/2 O_2 + 2 H^+ + 2 e^- \rightarrow H_2O$$ $E^o_{298 K}= 1.23$ V vs. SHE   [Eq. 1-5]

Net reaction:

$$HCOOH + 1/2 O_2 \rightarrow CO_2 + H_2O$$ $E^o_{298 K}=   1.45$ V   [Eq. 1-6]

In the direct formic acid fuel cell, dehydrogenation of formic acid (Equation 1-4) is the desired reaction pathway as opposed to dehydration pathway (Equation 1-7).

$$HCOOH \rightarrow CO + H_2O$$ [Eq. 1-7]

Anode catalyst selection is crucial in directing formic acid oxidation to proceed via the dehydrogenation reaction pathway (Equation 1-4). The second reaction pathway #2 (Equation 1-8 to 1-11) is similar to that of methanol oxidation, and forms adsorbed carbon monoxide as reaction intermediate (Rice & Masel, 2003).

$$HCOOH + Pt^o \rightarrow Pt\text{-}CO + H_2O$$ [Eq. 1-8]

$$Pt^o + H_2O \rightarrow Pt\text{-}OH + H^+ + e^-$$ [Eq. 1-9]

$$Pt\text{-}CO + Pt\text{-}OH \rightarrow 2 Pt^o + CO_2 + H^+ + e^-$$ [Eq. 1-10]

Overall: $HCOOH \rightarrow CO_2 + 2 H^+ + 2e^-$ [Eq. 1-11]
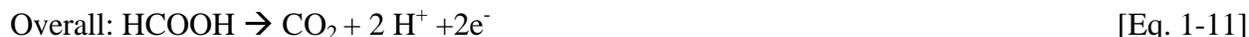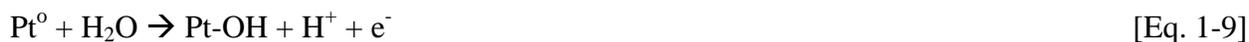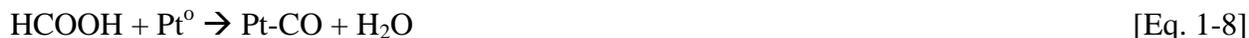
In reaction pathway #2, formic acid adsorbs onto the Pt surface forming an intermediate adsorbed CO species (Equation 1-8). Adsorbed OH groups (Equation 1-9) further oxidize the adsorbed CO intermediate into the gaseous CO_2 end product (Equation 1-10). For both the DMFC and DFAFC, carbon monoxide is formed as a reaction intermediate (Rice, Haa, & Masel, 2002).

However, CO adsorb strongly on Pt and lowers the electrochemically active surface area resulting in slower anodic kinetics. The accumulation of carbon dioxide gas is another challenge involved with DFAFCs and DMFCs that arises from the anode reaction product. The accumulated CO_2 gas would hinder the penetration of liquid fuel to the catalyst layer. To avoid the dehydration pathway, the DFAFC development has been more focused on Pd-based anode catalysts rather than Pt-based catalysts.

1.1 Theoretical background

Since in fuel cells system fuel and oxidant react to produce a useful electric energy output, a review of thermodynamic concepts related to reacting systems is important.

1.1.1 Electrochemical thermodynamics

Fuel cell converts the free-energy change of an electrochemical reaction into electrical energy. At constant temperature and pressure, the change in Gibbs free energy (ΔG) is the difference between the enthalpy change (ΔH) and the product of the change in entropy (ΔS) and temperature (Equation 1-12).

$$\Delta G = \Delta H - T\Delta S \qquad\qquad \text{[Eq. 1-12]}$$

In Equation 1-12, the change in enthalpy is the sum of the internal energy change and the mechanical work of a closed system as a result of volume change (Equation 1-13).

$$\Delta H = \Delta U + P\Delta V \qquad\qquad \text{[Eq. 1-13]}$$

According to 1st law of thermodynamic, the change in internal energy is equal to the amount of heat transferred into the system and the total work done by the system.

$$\Delta U = q - W \qquad\qquad \text{[Eq. 1-14]}$$

Based on the 2nd law of thermodynamics, the amount of the heat transferred can be set as $T \times \Delta S$ (reversible and closed system) and in electrochemical systems the total work done by the system is equal to the sum of the mechanical and electrical work.

$$\Delta U = T\Delta S - P\Delta V - W_e \qquad\qquad \text{[Eq. 1-15]}$$

By substituting Equation 1-13 and 1-15 in the Gibbs energy equation, the maximum electrical work for a reversible closed system can be defined as:

$$\Delta G^o = -W_e \text{ (at constant temperature and pressure)}$$

[Eq.1-16]

It is known that electrical work is the product of potential and total charge. Therefore, the Gibbs free energy can be related to the electrical potential via Equation 1-17; where $\Delta G < 0$ and $E > 0$ for a spontaneous process in a reversible electrochemical system.

$$\Delta G^o = -n \times F \times E^o$$ [Eq. 1-17]

Therefore, the standard free energy change expresses the tendency for any kind of process to occur under the conditions of constant temperature and pressure.

In Equation 1-17 above, the equilibrium potential of the system under the standard conditions (E^o) is related to the standard Gibbs free energy (ΔG^o) of the system by Faraday's constant (F), and the number of electrons transferred (n). Electrical work is done when an electric charge q moves through a potential difference of ΔV.

The value of ΔG^o expresses the maximum useful work that a closed system can do on the surroundings. This quantity of work ($-\Delta G^o$) can only be extracted from the system under the limiting conditions of a "thermodynamically reversible change", which for an electrochemical cell implies zero current. Therefore, the more rapidly the cell operates the less electrical work it can supply.

The standard Gibbs energy stated in Equation 1-17 is also related to the Gibbs free energy by the activities (a_i) of the system products, reactants, and temperature (T) as sown in Equation 1-18 below:

$$\Delta G = \Delta G^o + RT \ln \underbrace{(\Pi a_i^{S_i})}_{\text{Reaction Quotient}}$$

[Eq. 1-18]

In Equation 1-19, S_i is the stoichiometric coefficient of products and reactants that is positive for products and negative for reactants (Equation 1-19).The reaction quotient can be

calculated as the ratio of product activities raised to the power of their stoichiometric coefficient to the product of reactant activities raised to the power of their stoichiometric coefficient.

$$\sum_i S_i M_i + ne^- = 0 \qquad \text{[Eq. 1-19]}$$

From Equations 1-17 and 1-18, the cell potential can be related to the standard equilibrium cell potential through Equation 1-20, referred to as the Nernst equation.

$$E_e = E^o - \frac{RT}{nF} \ln\left(\Pi a_i{}^{S_i}\right) \qquad \text{[Eq. 1-20]}$$

In Nernst equation (Equation 1-20) for the gaseous compounds at low pressure, the chemical activity is equal to the gas pressure expressed in atmosphere, and at low aqueous reactant concentrations, the activity of substances can be expressed by their molar concentrations in solutions (Barbir, 2005).

Also, the effect of temperature variations on the cell performance should be taken into accounts when there are non-isothermal conditions exists. The effect of temperature on the equilibrium cell potential can be determined from the Maxwell equation (Equation 1-21).

$$\left(\frac{\partial \Delta G}{\partial T}\right)_p = -\Delta S \qquad \text{[Eq.1-21]}$$

Substituting Equation 1-17 into the Equation 1-21 gives Equation 1-22 which shows the relationship between the cell potential changes affected by temperature variations.

$$\left(\frac{\partial E_e}{\partial T}\right)_p = \frac{\Delta S}{nF} \qquad \text{[Eq. 1-22]}$$

Consequently, the overall equilibrium cell potential ($E_{e,cell}$) is the difference between the cathodic and anodic half-cell potentials (Equation 1-23) .

$$E_{e,cell} = E_{e,cathode} - E_{e,anode} \qquad \text{[Eq. 1-23]}$$

1.1.2 Kinetics of electrode processes

At fixed temperature, pressure, and equilibrium condition both reduction and oxidation reactions proceeds at equal rate at cathode or anode. Whereas, under non-equilibrium conditions, the oxidation reaction is dominant at the surface of the anode and reduction reaction is dominant at the cathode surface.

By definition, the current leaving the electrode is positive (i.e. anodic current) and the current coming into the electrode is negative (i.e. cathodic current).There are overpotentials (η) at the electrode related to electrode kinetics and mass transfer limitations that are responsible for a net loss in electrochemical systems.

$$\eta = E - E_e \qquad \text{[Eq. 1-24]}$$

The overpotentials increase with increase in current density being drawn from the system. Therefore, the actual cell potential becomes lower than the reversible cell potential due to irreversible losses. These irreversibilities which could be physical or chemical in nature are referred to as polarization. Hence, the actual cell potential and current curve is called polarization curve as shown schematically in Figure 1-3.
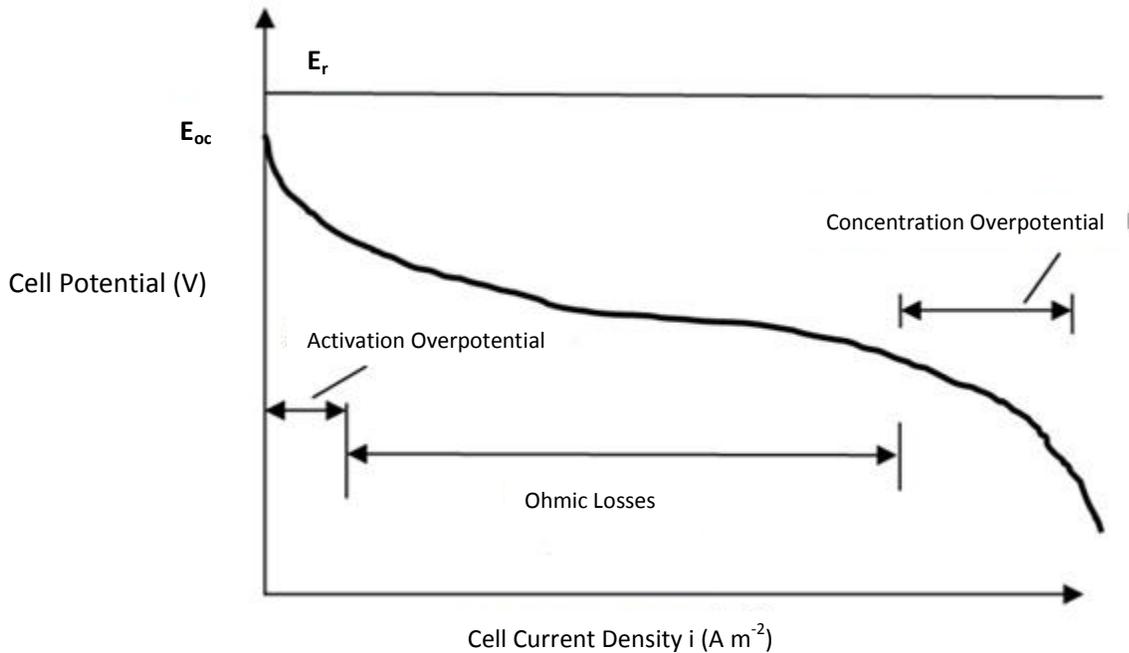
Figure 1-3: Cell polarization curve illustrating the idealized and actual cell potential-current relation with various forms of voltage losses (Blomen & Mugerwa, 1993)

There are different voltage losses associated with the actual operation of a fuel cell system. These voltage losses are categorized into three types of the activation losses (η_s), the Ohmic losses (η_c), and the concentration losses (η_c) that must be subtracted from the Nernst potential. Activation loss is due to the activation polarization that arises from the intrinsic electrode kinetics. Ohmic and concentration losses are caused by resistance to electrons/ions transport in the cell components, and mass transport limitations respectively.

The Buler-Volmer-Erdey-Gruz equation relates activation (surface) voltage losses to the cell current density by Equation 1-25.

$$i = i_o \left[\exp\left(\frac{\alpha_a F}{RT}\eta_s\right) - \exp\left(-\frac{\alpha_c F}{RT}\eta_s\right) \right] \qquad \text{[Eq. 1-25]}$$

Three parameters of anodic transfer coefficient (α_a), cathodic transfer coefficient (α_c), and the exchange current density (i_o) in Equation 1-25 are characteristics associated with the reaction and catalyst at the electrode. The transfer coefficients are independent of concentrations; whereas, the exchange current density (i_o) is strongly concentration and temperature dependent.

The Buler-Volmer-Erdey-Gruz equation can be simplified under conditions of large and small over potentials. That is, at high negative over potentials (e.g. $\eta < -0.1V$), the equilibrium is shifted towards the forward direction (Equation 1-26).

$$|\eta_s| = b \, log\left(\frac{|i|}{i_o}\right) \; ; b = \frac{2.303 \, R \, T}{|\alpha*|F} \qquad \text{[Eq. 1-26]}$$

In equation 1-26, $|\alpha*|$ can be defined as α_a for anodic reaction and $-\alpha_c$ for cathodic reaction

The original Butler-Volmer-Erdey-Gruz (Equation 1-25) can further be approximated by a two term Taylor series expansion (Equation 1-27).

$$i = i_o \frac{(\alpha_a + \alpha_c)}{RT} F\eta_s = i_o \frac{nF}{RT}\eta_s \qquad \text{[Eq. 1-27]}$$

To understand the losses associated with concentration gradient, one must consider a thin diffusion layer of thickness (δ) adjacent to the electrode surface.
The current density related to surface concentration of reactants can be modeled by Nernst diffusion layer equation (Equation 1-28).

$$i = \frac{-nFD \, (c_b - c_s)}{\delta} \qquad \text{[Eq. 1-28]}$$

In which, D is the effective diffusion coefficient.

For a given electrode, c_b is fixed and i increase as c_s become smaller. When the concentration of reactants at the electrode surface is depleted ($c_s=0$), the rate of reactant diffusion

to the electrode surface from the bulk solution is not high enough; therefore, the mass transfer limiting current density becomes:

$$i = \frac{-nFDc_b}{\delta} \qquad \text{[Eq. 1-29]}$$

Any further attempt to increase the current from the system cannot be supported by the limited rate of reactant transport and therefore, the limiting condition for the current density drawn will be achieved. Hence, the concentration overpotential can be related to limiting current density by Equation 1-30.

$$\eta_c = \frac{RT}{nF} \ln\left(1 - \frac{i}{i_L}\right) \qquad \text{[Eq. 1-30]}$$

Electricity in a fuel cell is transported through the electronically conducting solid components by flow of electrons and through liquid or solid ion conductors by transport of ions. Therefore, the Ohmic losses caused by the electrical resistance in cell components must be accounted in the overall cell voltage calculations. The Ohmic drop ($\Delta\varphi_{ohm}$) is associated with internal electrical resistance, which includes the ionic and electronic resistances. The ion transport between the cell components can be related to the electrolyte conductivity (κ) and electrode spacing (d) by Equation 1-31.

$$\Delta\phi_{ionic} = \frac{id}{\kappa} \qquad \text{[Eq. 1-31]}$$

In the fuel cell, the electronic losses are almost negligible and resistance is primarily caused by ionic (electrolyte) resistance (Barbir, 2005).

Taking into account all types of cell losses, the fuel cell performance can be calculated by subtracting the losses from the equilibrium cell potentials (Equation 1-32).

$$E_{actual} = E_e + \eta_{s,\,cathode} - \eta_{s,\,anode} + \eta_{c,\,cathode} - \eta_{c,\,anode} - \Delta\varphi_{ohm} \qquad \text{[Eq. 1-32]}$$

1.1.3 Half-cell potential and reference electrode

To measure the change in potential difference in the fuel cell system, it is necessary to include a stable reference electrode which acts as a half-cell. The most conventionally used

reference electrode is the standard hydrogen electrode (SHE), which is defined to be 0 V. The SHE is based on the hydrogen redox reaction at standard condition and temperature of 298 K shown in Equation 1-33:

$$2H^+ + 2e^- \rightarrow H_2 \qquad\qquad\qquad \text{[Eq. 1-33]}$$

The purpose of the reference electrode is to complete the measuring circuit and provide a stable and reproducible potential against which the working electrode is compared. The electrode reactions are very fast in both directions and the standard reference electrode has a negligible over potential when a small current is drawn from them system. However, the hydrogen reference electrode requires constant gas supply that makes it inconvenient in measurements. Hence, there are several other reference electrodes available commercially such as Hg/Hg_2Cl_2 and $Ag/AgCl$ in saturated KCl electrolyte.

The most common and simplest reference system is the silver/silver chloride single junction reference electrode. This generally consists of a cylindrical glass tube containing a 4 molar solution of KCl saturated with AgCl (Barbir, 2005).
 In electrochemical terms, the half-cell can be represented by:

$$Ag / AgCl_{(Satd)}, KCl_{(Satd)} \qquad\qquad\qquad \text{[Eq. 1-34]}$$

and the electrode reaction is:

$$AgCl \text{ (s)} + e^- = Ag \text{ (s)} + Cl^- \qquad\qquad\qquad \text{[Eq. 1-35]}$$

The electrode potential for above half-cell is + 0.204 V relative to the standard hydrogen electrode (SHE) at 298 K. On the other hand, the chloride based reference electrodes can be problematic in conjunction with Pt-based working electrode. Since there is a possibility of Cl^- poisoning of Pt, the mercury-mercurous sulphate electrode in an aqueous K_2SO_4 electrolyte can be used. The reaction in the mercury-mercurous sulphate electrode is given in Equation 1-36.

$$Hg_2SO_4 + 2e^- \rightarrow 2Hg + SO_4^{2-} \qquad\qquad\qquad \text{[Eq. 1-36]}$$

1.1.4 Experimental methods for electrode kinetics studies

Typically a three-electrode setup consisting of a working electrode, a counter electrode, and a reference electrode is employed for electrode kinetic studies (Figure 1-4). In this setup, the potential of the working electrode is measured against a reference electrode of choice. Electrochemical methods such as cyclic voltammetry (CV), chronopotentiometry (CP), and chronoamperometry (CA) are commonly conducted to obtain specific characteristics of working electrode.
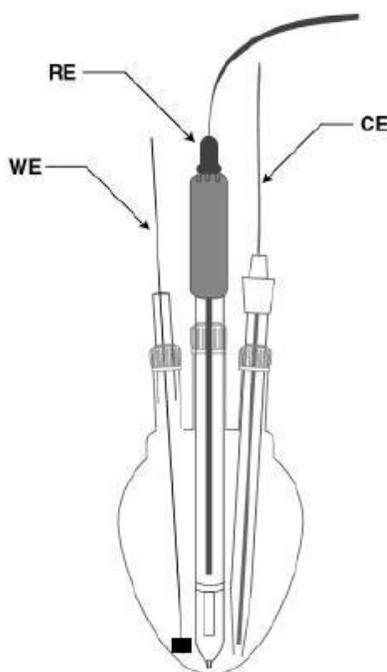
Figure 1-4: Three electrode set-up for electrochemical testing (Wang J. , 2006).

1.1.5 Cyclic voltammetry

The most used technique in electroanalytical studies is the cyclic voltammetry which consist of scanning linearly the potential of the working electrode against time at a specific scan rate (V_s) (Wang J. , 2006). Typically, the potential is linearly changed from an initial set value (E1) to an end value (E2) and back again. The current produced is measured and plotted against the voltage which is termed as cyclic voltammogram graph (Figure 1-5). Depending on electrode

characteristic, single or multiple cycles and different scan rates can be used. The expected response of a typical redox reaction is illustrated in Figure 1-5.
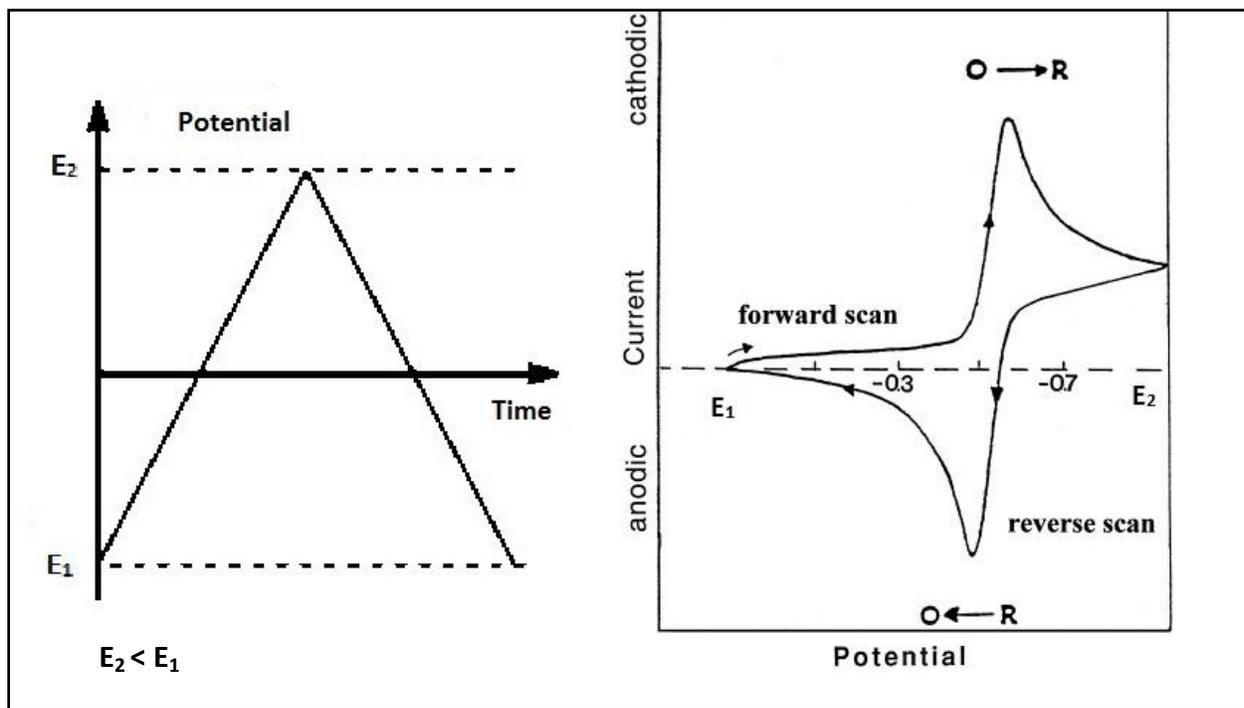
Figure 1-5: Cyclic voltammetry response signals (Bard & Faulkner, 2001).

At the beginning of the cycle, it is assumed that only the oxidized species (O) are present and therefore a negative-going potential scan is applied (Figure 1-5). As the applied potential approaches the E^o for the redox process, the cathodic current increases until a peak is reached. In the second part of the cycle, the scan is reversed and R molecules (generated in the forward scan) are re-oxidized back to (O) to generate anodic current.

Thus, at diffusion controlled the peak current (i_p) is given by Randles-Sevcik equation (Equation 1-37) (Bard & Faulkner, 2001).

$$i_p = 0.4463 \text{ nFAC} \left(\frac{nFv_sD}{RT}\right)^{1/2} \qquad \text{[Eq. 1-37]}$$

15

For an irreversible reaction the Equation 1-38 which is derived from Randles-Sevcik equation can be used (Wang J. , 2006).

$$i_p = 0.4961 \; nFAC \left(\frac{\alpha n^* F \nu_s D}{RT}\right)^{1/2} \qquad\qquad \text{[Eq. 1-38]}$$

In which, α is the charge transfer coefficient, and n* is the number of electrons transferred in the rate determining step.

1.1.6 Chronopotentiometry

Chronopotentiometry is an electrochemical technique in which a controlled current, (usually a constant current) is applied between two electrodes .The potential of one electrode is monitored as a function of time against the reference electrode. A typical current density-time curve and potential-time curve are illustrated in Figure 1-6. When the constant current is applied through the cell (between the working and auxiliary electrodes), at the beginning the working electrode potential increases rapidly due to the charge build up at the electrode/solution interface. The working electrode potential varies over the time as shown in Figure 1-6, b.
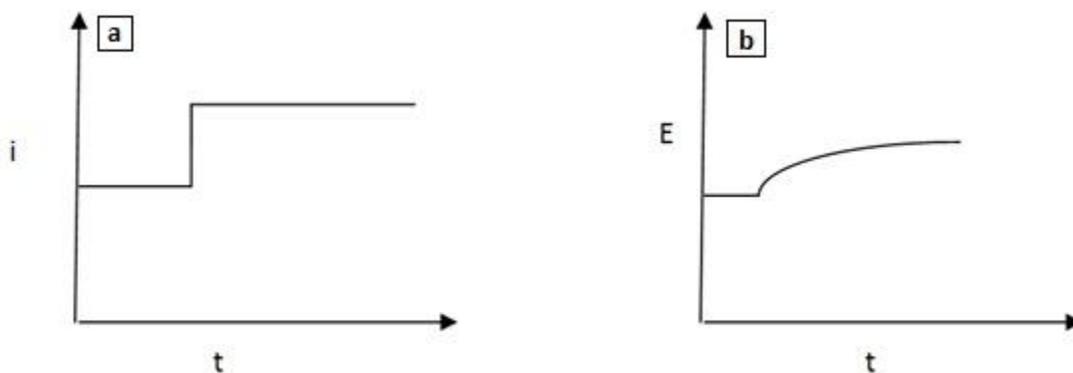
Figure 1-6: Chronopotentiometry response signals (Bard, et al., 2001).

From chronopotentiometry, the stability of electrode over time can be determined. A stable electrode should remain at a relatively constant potential over time. The deviations observed in potential correspond to catalyst poisoning, changes in electrode or electrolyte characteristics, and concentration.

1.1.7 Chronoamperometry

Chronoamperometry is a half- cell electrochemical technique which is conducted in a tri-electrode setup. In this method, potential is fixed between the working and reference electrode and total cell current is measured for specific time. Typical chronoamperometry plots are illustrated in Figure 1-7; where, the voltage is stepped up from an initial voltage value (e.g. open circuit voltage) at t_0. The current-time relationship after $t=t_0$ is based on the Cottrell equation (Equation 1-40) which defines current-time dependence for linear diffusion control. The linear relationship between the current (i) and $t^{-1/2}$ is referred as the Cottrell graph. When the current-time relationship does not follow the Cottrell plot, chronoamperometry can be applied to determine the Tafel slope in kinetic regime.

$$i = nFC_o \sqrt{\frac{D}{\pi.t}}$$
[Eq. 1-40]
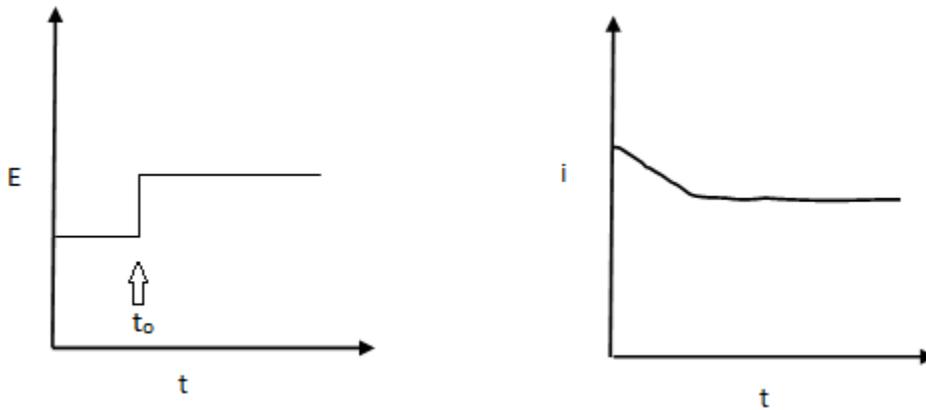
Figure 1-7: Chronoamperometry response signals (Bard, et al., 2001).

2.0   Literature review

2.1   Formic acid oxidation

It is believed that the electro-oxidation of formic acid on Pt group metals follows a dual-pathway consisting of a non-CO_{ads} direct and a CO_{ads} indirect mechanism originally suggested by Capon and co-workers (Capon & Parsons, 1973). The electro-oxidation mechanism of formic acid on Pd involves dehydrogenation and direct formation of CO_2 known as the direct-pathway. Whereas, the indirect-pathway involves the formation of intermediates such as CO which depends on the electrode potential followed by the oxidation of these intermediates to CO_2 (Capon & Parsons, 1973).

Okamoto et al., studied the behaviour of formic acid electro oxidation via cyclic voltammetry experiments (Figure 2-1). In Figure 2-1, peak 1 is associated with the dehydrogenation of formic acid and the formation of CO_{ads} on the surface. Whereas, peak II corresponds to the oxidation of CO_{ads} and subsequent formation of surface oxide/hydroxide. Peak III is associated to dehydrogenation process of formic acid on the oxide surface. On the reverse scan, peak IV is attributed to the oxidation of formic acid on clean surface (Okamoto, Kon, & Mukouyama, 2005).
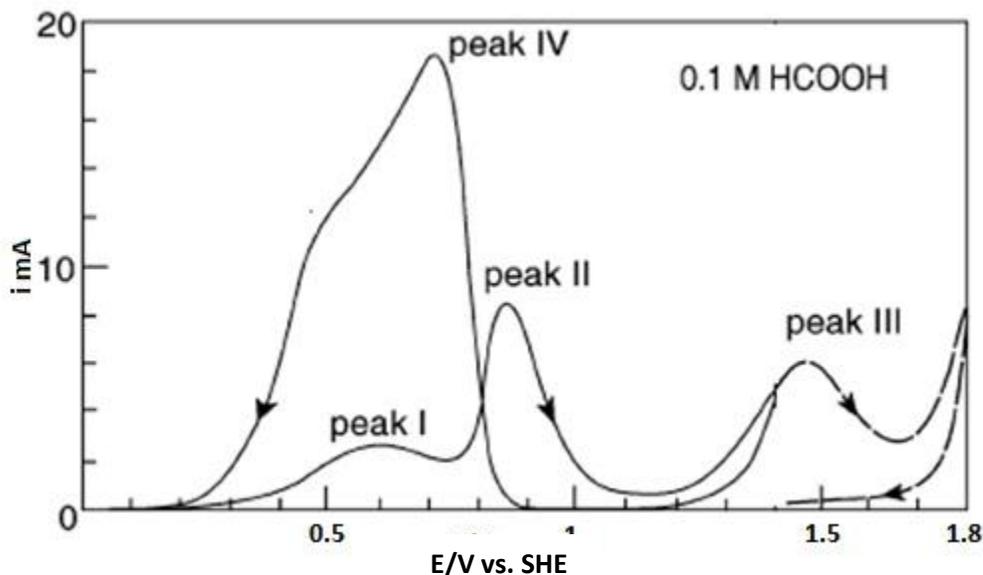
Figure 2-1:Cyclic voltammogram of formic acid electro-oxidation on Pt surface in 0.1 M HCOOH and 0.5 M H_2SO_4 at 315 K (Okamoto et al, 2005).

It is believed that the electro-oxidation of formic acid on Pd-based anode catalysts proceeds via the direct non-CO_{ads} pathway especially at low potentials (<0.4 V vs. SHE) (Rice & Masel, 2003; Zhu & Uchida, 1999).

 Larsen and coworkers, studied the CO build up on Pd black by stripping voltammetry and showed the CO build up on the surface of Pd black was lower compared to the surface of Pt black (Larsen, Zakzeski, & Masel, 2006). As a result, Pd-based anode catalysts are catalytically more active towards the electro-oxidation of formic acid than Pt, especially at potential range lower than 0.4 V vs. SHE within which adsorbed CO intermediate cannot be oxidized on the surface of Pt (Arenz, & Schmidt, 2003; Blair & Lycke, 2006).

In comparison to Pt, Pd anode catalysts suffer an unacceptable loss of performance with time that drops the cell's power density by half in a few hours. Pd is very active at lower potentials around 0.4 V in contrast to Pt , but the weakly adsorbed CO intermediates on the surface decreases the catalytic activity of Pd within a very narrow potential region. The deactivation of Pd in short time has been investigated by many researchers (Blair & Lycke, 2006; Li & Hsing, 2006; Choi, 2008).

Blair & Lycke., studied the long term stability of both Pd and Pt catalysts at 293 K. Results indicated higher catalytic activity of Pd at the initial hour of operation which falls quickly below Pt and that of Pd-Pt activity within hours. According to the cyclic voltammetry tests, (Figure 2-2) the sharp drop of performance above 0.4 V vs. SHE is associated with pure Pd; whereas, in the case of Pt the maximum activity falls around 0.6 V vs. SHE (Blair & Lycke, 2006).

 At potentials higher than 0.6 V vs. SHE, Pt activity declines as the dissociated water on Pt mitigates the build-up of poisoning intermediates via formation of oxidizing species on the catalyst surface (Li & Hsing, 2006). Another explanation of fast deactivation of Pd performance at high voltages is likely a result of Pd dissolution and the adsorption of intermediate species such as H_{ad}, OH_{ad} or Pd oxides that blocks the available active site (Li & Hsing, 2006).
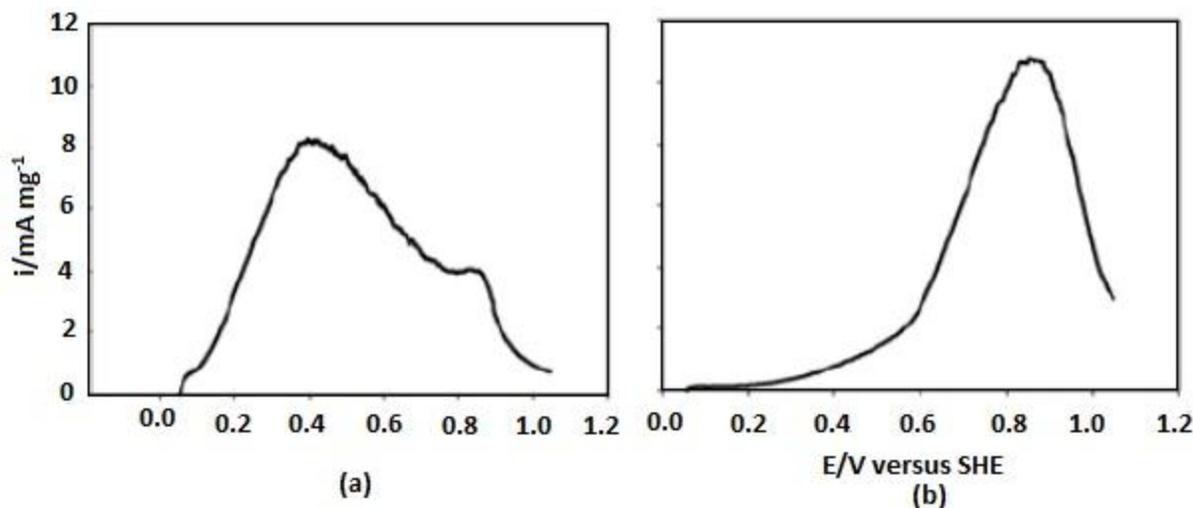
Figure 2-2: Electro-oxidation of HCOOH on (a) Pd;(b) Pt at 293 K; 0.1 M H$_2$SO$_4$ and 0.1 M HCOOH; scan rate of 5 mV s^{-1}) (Blair & Lycke, 2006).

In regards to performance improvement of Pd and Pt anode catalysts, incorporating bimetallic catalysts including Pt-Ru, Pt-Pd and Pd-Sn have been studied by various researchers (Li & Hsing, 2006; Arenz et al, 2003; Blair & Lycke, 2006). A comparison between Pt-Ru and Pt-Pd shows higher catalytic activity of Pt-Ru andoe at large current density as a result of different reaction mechanism. Larsen and co-workers suggested that formic acid electro-oxidation proceeds via a non-CO$_{ads}$ pathway in the case of Pt-Ru (Larsen et al, 2006). While Pt-Pd anode experienced the same deactivation problem as pure Pd , Pt-Pd exhibited better long term stability (Rice & Masel, 2003).

Kang, et al., studied Pt anode modification by incorporating Bi into catalyst layer and prepared Pt-Bi anode catalyst by under potential deposition (UPD) method. The positive enhancement of catalytic activity due to addition of Bi adatoms on Pt catalyst was explained by third-body effect and an electronic effect on a single crystalline Pt surface. In CV experiments (Figure 2-3), the Pt electrode modified by Bi suppressed the hydrogen adsorption and therefore increased the oxidation current (Kang, Lee, & Chung, 2006).
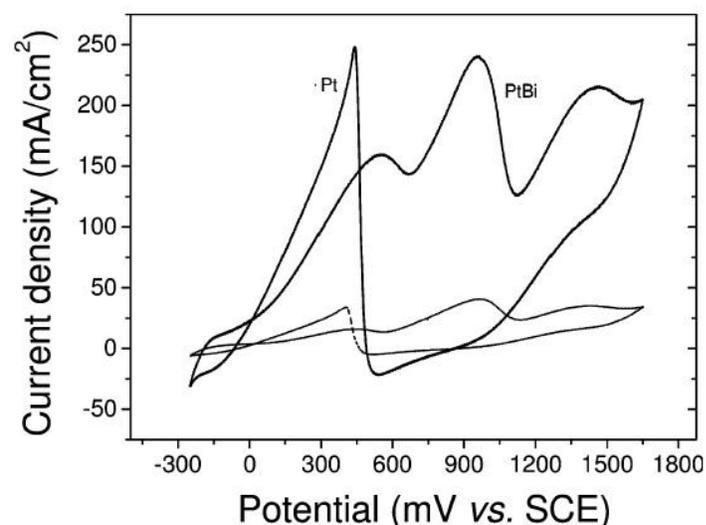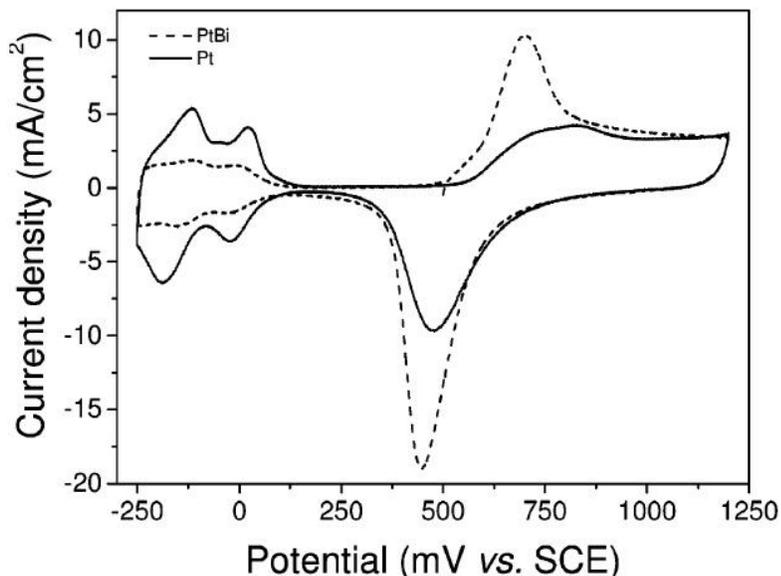
Figure 2-3: (a) Cyclic voltammogram of Pt and Pt-Bi in 1.0 M HCOOH,0.5 M H$_2$SO$_4$ at scan rate of 50 mV s^{-1} and 298 K ;(b) cyclic voltammogram of Pt and PtBi in 0.5 M H$_2$SO$_4$ at scan rate 50 mV s^{-1} and 298 K(Kang et al, 2006).

Superior catalytic activity of Pd-based catalysts due to their ability to overcome the CO poisoning effect also makes Pd and Pd bimetallic anode catalysts the topic of research in many studies.

To improve the electrocatalytic performance of Pd, Haan et al., investigated the positive effect of PdSn/C on formic acid oxidations. Results indicated superior DFAFC performance in case of PdSn/C due to the third-body effect (Figure 2-4). It is believed that the formation of adsorbed CO is prevented on Pd catalyst surface by addition of Sn particles. A comparison of four different Pd-based anode catalysts in the direct formic acid fuel cell is shown in Figure 2-4 (Stafford, Richard, & Haan, 2010). The superior catalytic activity of PdSn/C catalyst is evident from polarization curves compared with pure Pd/C catalyst (Haan et al, 2010).
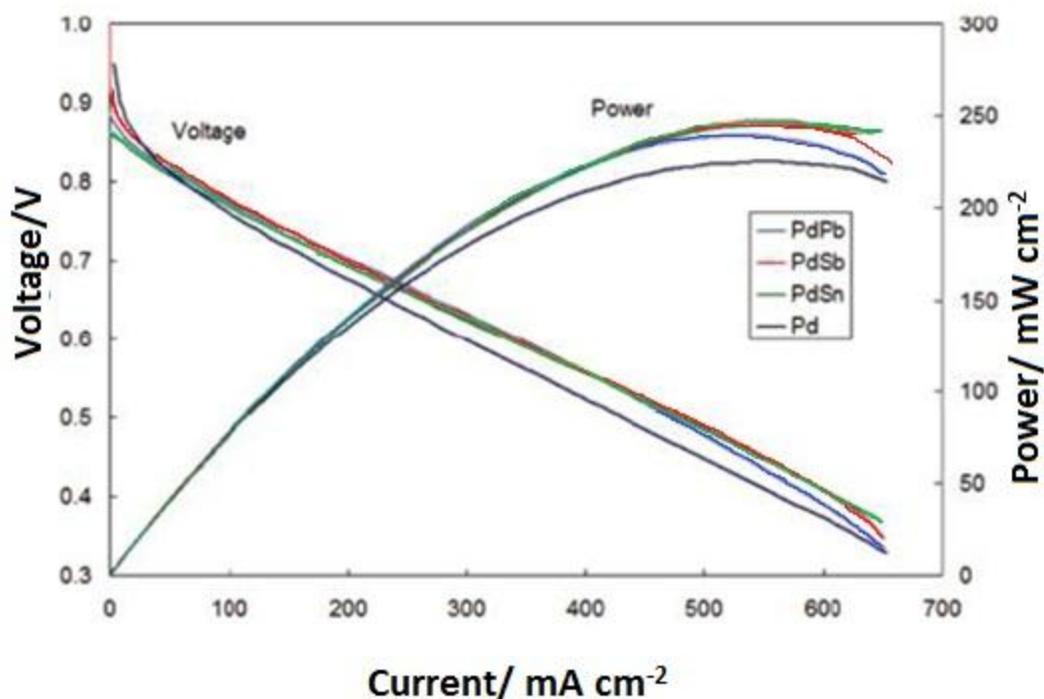
Figure 2-4:Pd-based anode catalysts in DFAFC operating at 303 K and 10 M formic acid flow at 1 mL min^{-1} (5 cm^2 geometric area) on the anode; air flow rate of 300 ccm (Haan et al, 2010).

In agreement with Haan et al., similar study by Liu and co-workers confirmed the positive effect of adsorbing Sn onto Pd/C carbon black. Liu & Xinhu, investigated the effect of Sn incorporated with Pd. Performance comparison in DFAFC test between pure Pd/C and PdSn/C bimetallic electrocatalyst indicated the positive effect of Sn in enhancement of formic acid oxidation and reduction of CO poison on the catalyst surface (Liu & Xinhu, 2009). Results found suggested, PdSn/C catalyst was weakening the adsorption strength of CO on Pd through electronic effects and thereby enhances the overall catalytic activity (Liu & Xinhu, 2009). Based on co-stripping linear sweeping voltammograms conducted by Liu & Xinhu., no anodic peak appeared on the Sn/C catalyst that indicated no CO adsorbed on the Sn surface (Figure 2-5).
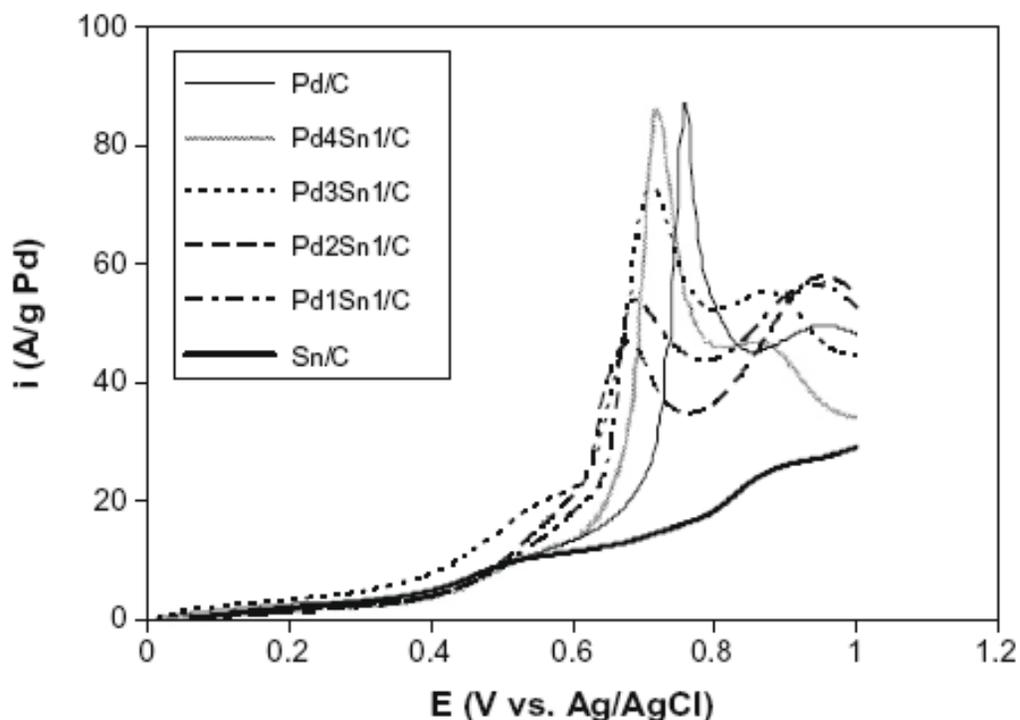
Figure 2-5: Co-stripping linear sweeping voltammograms of Pd/C and PdSn/C catalyst in 1 M HCOOH ,0.5 M H$_2$SO$_4$ at 298 K with scan rate of 50 mV s^{-1} (Liu & Xinhu, 2009).

Markovic et al., studied the Pt-Ru bimetallic catalyst in oxidation of formic acid and emphasized on the electro-oxidation of formic acid via the dehydration pathway. The ability of Ru to provide nucleating oxygen containing sites to oxidize adsorbed carbonaceous species at lower voltage than Pt promotes the catalytic activity of Pt-Ru compared to pure Pt (Markovic & Gasteiger , 1995). In agreement with Markovic & Gasteiger, Rice and co-workers demonstrated the superior Pt-Ru catalytic activity among Pt and Pt-Pd catalysts at high current density illustrated in Figure 2-6 (Rice & Masel, 2003).
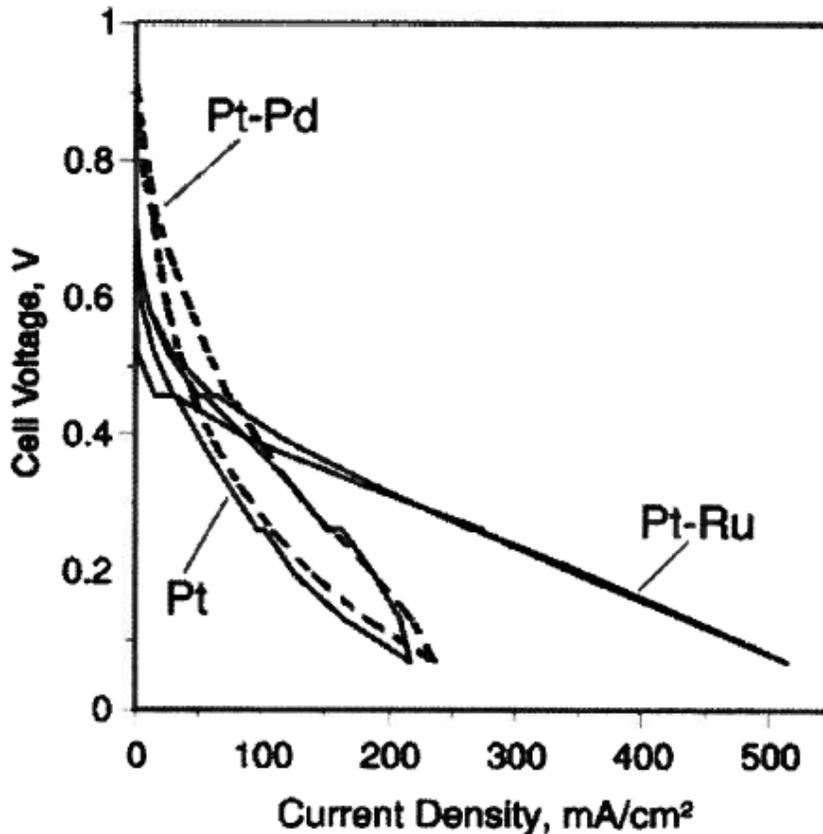
Figure 2-6: Polarization curves for DFAFC at 303 K including Pt, Pt-Ru and Pt-Pd anode catalyst with 40 g m^{-3} load. Fuel feed: 5 M HCOOH fed at 0.5 ml min^{-1} and 70 g m^{-2} Pt black cathode (5 cm^2 geometric area);O$_2$ flow rate of 100 sccm and back pressure of 30 psi at standard condition (Rice & Masel, 2003).

2.2   Surface activation of carbon fiber

The widespread use of carbon based material in electrochemical systems started around 1840s. The development of artificial graphite that was first used for anodes in Chlor-Alkali cells, led to a rapid growth of industrial electrochemical processes (Campanati & Fornasari, 2003). Carbon supported catalysts are preferable support as they provides high catalyst dispersion and good electronic conductivity (Langer & Tri, 1993).

Also, due to the characteristics such as low density, high purity, adequate corrosion resistance, availability and low cost, carbon is a good material for 3-D electrodes to be employed in PEMFCs. Different structures of carbon in forms of carbon paper, carbon felt, cloth, and

powder are used in variety of electrochemical systems. Carbon black in the form of fine powder has been conventionally used as the electrocatalyst support and gas diffusions electrodes (GDE) (Barbir, 2005).

2.2.1 Carbon fiber activation and treatment methods

The efficiency of catalyst deposition depends on the state of the fiber surface and its morphology. In the case of carbon fiber material, the surface functional groups within carbons are responsible for the variety of physiochemical and catalytic properties (Li, Ma, & Lu, 2005).

Modification of surface functional groups by liquid chemical oxidation solutions such as nitric acid, sulfuric acid, and hydrogen peroxide is widely practiced. Among all the different functional groups, the oxygen-containing functional groups (surface oxides) are the most common species formed on the carbon fiber surface. These surface oxides influence the catalytic and adsorption characteristics of carbon (Shen, Li, & Liu, 2008). Liquid acid treatment is mostly applied to oxidize the carbon fiber surface to enhance the acidic properties and hyrophilicilty of carbonous surface. Nitric acid and sulphuric acid were the most commonly used acid solutions in activation of carbon surface (Shen et al, 2008).

Wu et al., studied the effect of nitric acid and sodium hydroxide treatment on surface properties of carbon fiber (Wu, U, & Pittman, 1995). The process of nitric acid oxidation and sodium hydroxide treatment produces acid groups and replaces H^+ of surface acid groups by Na^+ respectively. It is found that the acidic capacities of carbon fiber increased linearly with nitric acid concentration and treatment time. In the case of carbon felt material, etching of thick carbon felt (3 mm thickness) substrates in a concentrated (98%) H_2SO_4 and potassium dichromate solution at 298 K is practiced by Kinoshita. It is known that etching of carbon felt leads to simultaneous appearance of –C=O and –C-O groups involved in redox processes of formation of primary metal crystallization centers (Kinoshita, 1988).

Li et al., studied the effect of nitric acid concentration on activated carbon on supported Pd catalyst. Activated carbon was pre-treated separately in various concentration of nitric acid (from 0.5 to 67 wt%) at $95^{\circ}C$ for Pd catalyst support (Li et al, 2005). Figure 2-7 shows the TEM pattern of Pd catalyst support pre-treated in different nitric acid concentrations. Comparing the Pd catalyst support pattern in Figure 2-7 along with XRD analysis indicated enhanced Pd

dispersion within dilute nitric acid concentration range (<10 wt%). Whereas, pre-treatment at higher concentrations resulted in forming dense oxygen surface groups and increased in total acidity environment by 13 times compare to untreated surface (Li et al, 2005).
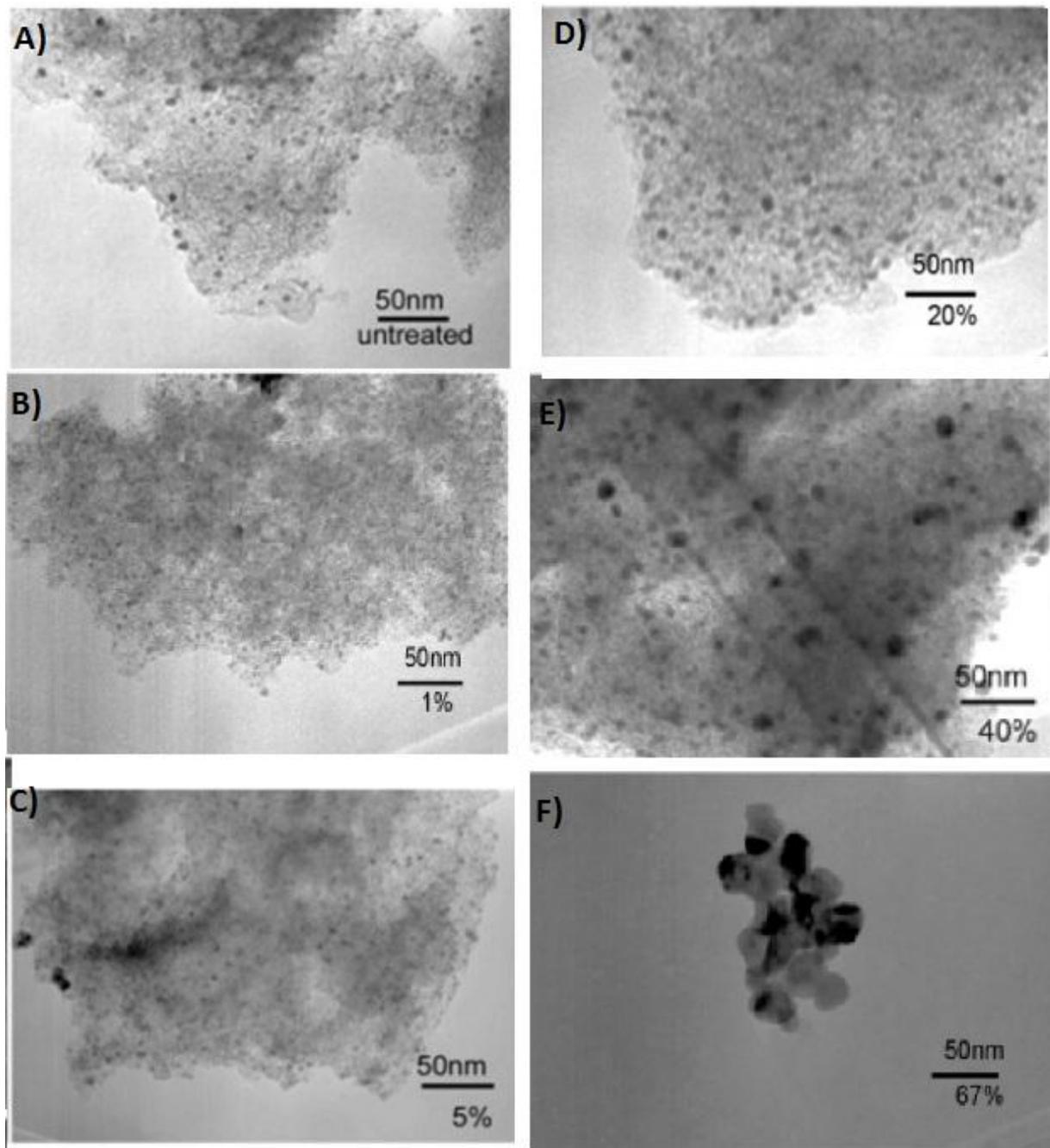
Figure 2-7:TEM micrographs of Pd/C catalysts. Impact of increasing nitric acid concentration on Pd dispersion on activated carbon surface at 368 K for 5 hours pre-treatment period (Li et al, 2005).

Another activation method for enhancement of Pd catalyst coverage with adequate adhesion is treatment in solutions containing Sn species. Tin/palladium solution has been widely applied to activate non-conductive surfaces. Cheng and Gyenge, studied the effect of a mixed tin/palladium solution known as Shipley-type solution in activating carbon felt surface (thickness 3 mm) (Cheng & Gyenge, 2009). When using a mixed Pd-Sn activator acid solution , a complex between Sn(II) and Pd(II) is initiated followed by reduction of the Pd(II) to Pd(0) that forms a nucleus for the growth of the colloid (Horkans, 1983). During the sensitization step of carbon material, colloidal particles of Sn (II) adsorb on the surface of carbon. The Sn(II) particles act as catalytic sites in the reduction of the Pd^{2+} according to following (Cheng & Gyenge, 2009).

$$Pd^{2+} +Sn(II) \rightarrow Pd^0 +Sn (IV) \hspace{3cm} [Eq. 2-1]$$

2.3   Anode structure design in direct liquid fuel cell

Various electrode designs have been researched in literatures including novel porous carbon catalyst supports (Kinoshita, 1988). The concept of extended reaction zone anode (also called three dimensional electrode) for DMFCs have been demonstrated by Bauer and co-workers. Compared to conventional anode structure design, the high surface area support material has enhanced cell performance by providing uniformly distributed catalyst nanoparticles throughout the electrode thickness. Figure 2-8 represents the high resolution SEM images of naked compressed felt and catalyzed compressed felt (Bauer, Gyenge & Oloman, 2006). Pressed, uncompressed graphite felts and reticulated vitreous carbon have been investigated as
 3-D electrode materials in DMFC and DFAFC systems (Cheng & Gyenge, 2009) . In a study conducted by Bauer and co-workers on three-dimensional electrodes, the positive effect of 3-D anode design on the performance of DMFC compared to conventional gas diffusing electrode was observed. With the same Pt loading, the DMFC performance improved by 38% with the novel 3-D electrode (graphite felt) at 3000 A m^{-2} and 333 K (Bauer, Gyenge & Oloman, 2007). The enhanced performance could be likely attributed to the higher utilization of nanoparticle catalyst.
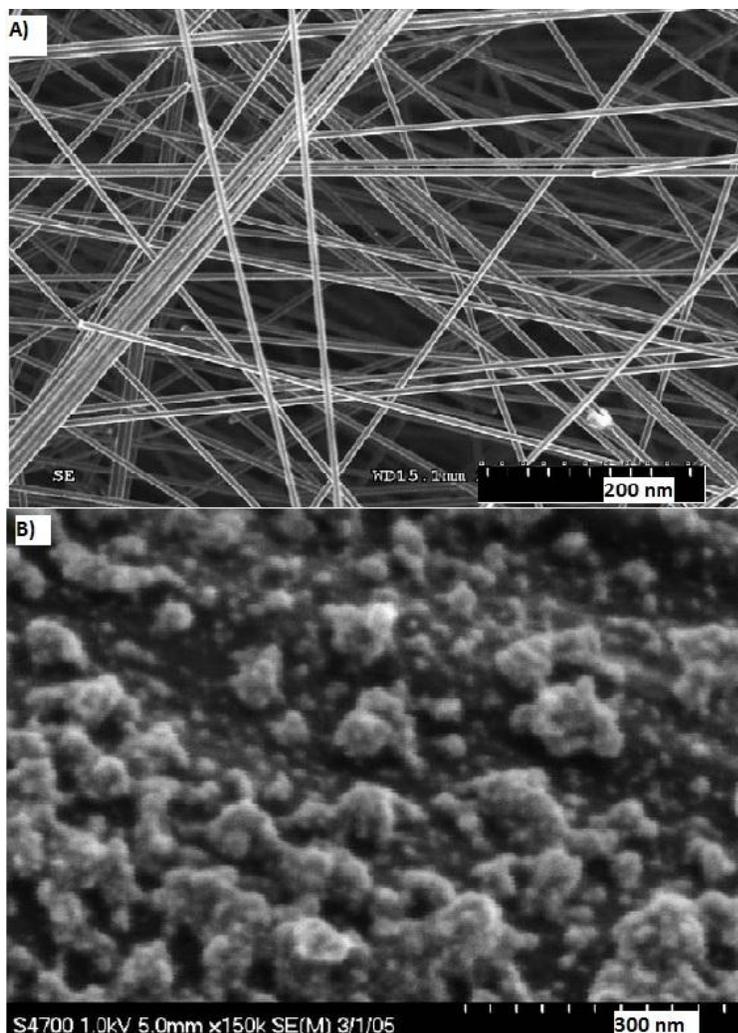
Figure 2-8: High resolution SEM micrographs on compressed fell (0.3 mm thickness);(a) naked compressed felt ;(b) Pt-Ru deposited on the compressed graphite felt surface (Bauer et al, 2006).

The alternative anode designs include supports such as titanium mesh (Allen et al, 2005) and carbon nanotubes (Chan, Yong, & Takashi , 2004) that generally provide significant improvement in cell performance compare to conventional anode designs.

Shao et al., electrodposited Pt-Ru catalysts onto titanium mesh as the 3-D anode (Shao et al, 2006). The superior DMFC performance compared to systems operating on conventional catalyst is evident at high current densities and 0.5 M methanol concentration in Figure 2-9.

The reason for enhanced DMFC performance at high current density is due to the good catalyst utilization and better methanol mass transport as well as CO_2 (g) disengagement. One

major drawback from this design was the severe methanol crossover at 2 M methanol concentration due to the open titanium mesh structure in this design (Shao et al, 2006).
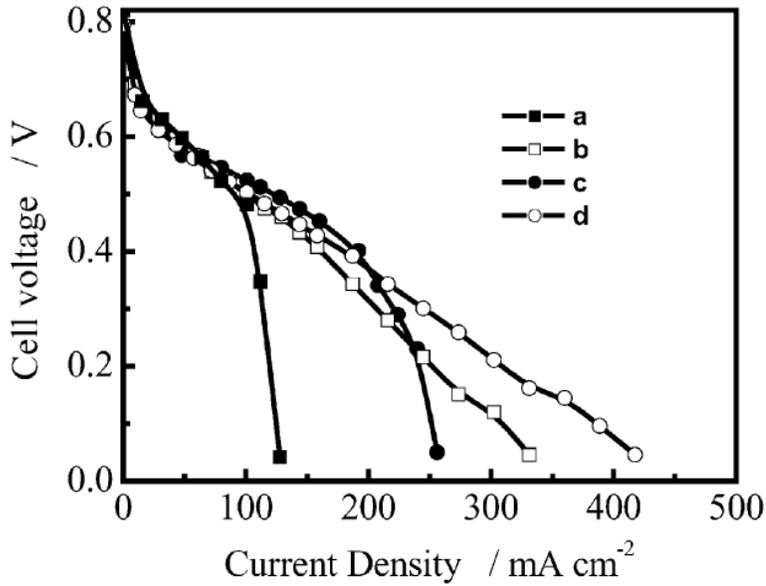
Figure 2-9: Comparison of the performance of the DMFC with different anode structures at 368 K with atmospheric oxygen gas feed: (a) 0.25 M methanol, conventional anode; (b) 0.25 M methanol, PtRu/Ti anode ;(c) 0.5 M methanol, conventional anode;(d) 0.5 M methanol,PtRu/Ti anode (Shao, Zhu, Lin, & Christensena, 2006).

3.0 Objectives

Porous three-dimensional electrodes are promising candidates for use in DFAFCs. It is believed that the extended reaction zone in the three-dimensional electrodes allows formic acid to react more completely in the anode; and therefore, leaving less fuel crossover within the system. Figure 3-1 illustrates the position and structure of 3-D electrode in DFAFC.

There has been very limited research done on direct deposition of catalyst particles throughout the 3-D electrodes and most literature studies were focused on electrodeposition rather than the electroless deposition technique.
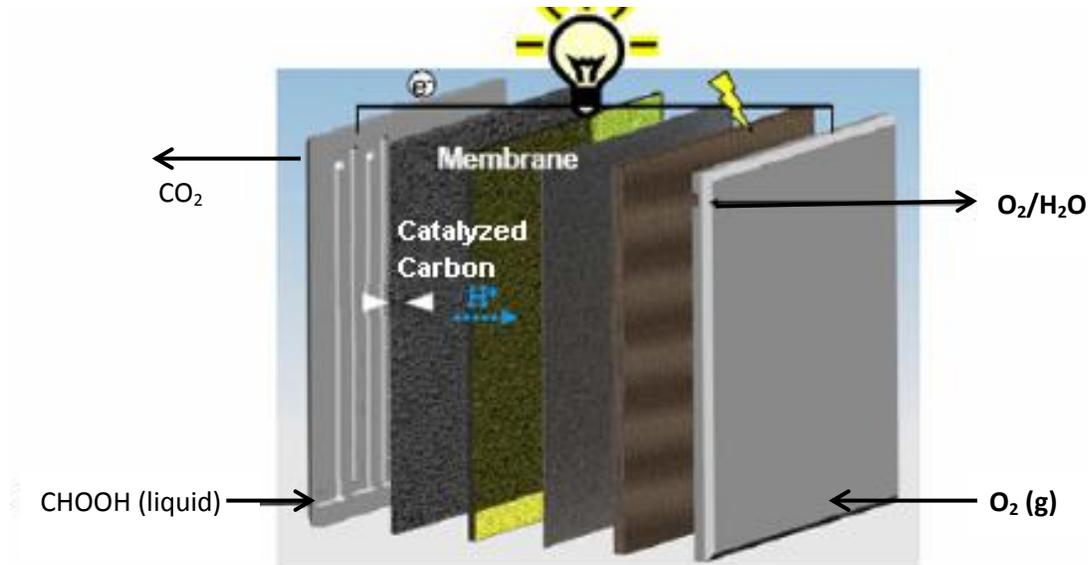
Figure 3-1: Exploded view of DFAFC with 3-D extended reaction zone anode (Bauer et al, 2009).

The catalyst preparation method employed in the present study is electroless or chemical deposition. The technique of electroless catalyst deposition could be advantageous method over electrodeposition in synthesizing of catalyzed electrodes due to its low cost, simple equipment set-up and uniform particle deposition characteristics.

To successfully deposit catalyst particles from their salts, the electroless solution must include various chemicals such as reducing agent, stabilizer and complexing agents. In addition Nafion® (5 wt%) perfluorinated resin solution is used in the chemical bath as an additive.

Investigation of the Nafion® effect on catalyst loading and surface morphology of the 3-D substrate (AvCarb P50 ^{TM}) is novel. AvCarb P50 ^{TM} (carbon fiber material) is chosen as the support due to its porous surface characteristics and thickness of 175 microns that reduces the Ohmic losses in cell performance (Figure 3-2). Therefore, the main objectives of this study include the investigation of electrocatlytic activity of the novel catalyzed three-dimensional substrate for the oxidation of formic acid and analysis of substrate surface morphology in terms of catalyst loading and particle size. Also, to develop an easy to use method for Pd and Pd-Sn catalysts deposition on carbon material substrates, and to investigate the effect of Nafion® solution used in the electroless bath on the carbon substrate surface morphology.
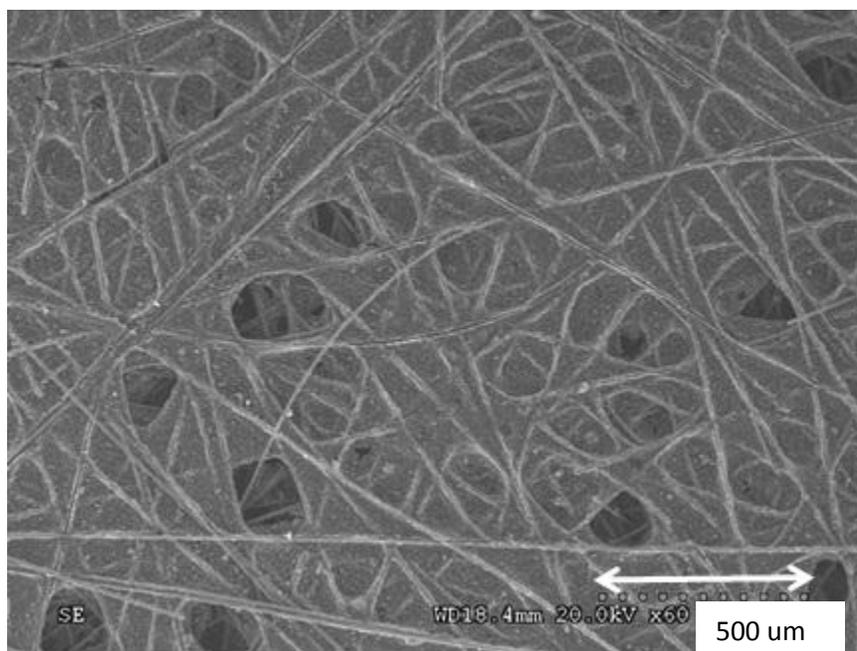
Figure 3-2: High resolution micrograph of AvCarb^{TM} P50 electrode material with the approximate thickness of 175 microns.

4.0   Experimental methods

Experimental methods conducted in current study consisted of: a) electroless catalyst deposition, b) surface morphology analysis (SEM and ICP-MS analysis), c) half-cell experiments including cyclic voltammetry, chronoamperometry and, d) fuel cell polarization experiments.

4.1   Electrode material

The carbon fiber material (AvCarb^{TM} P50) chosen as catalyst substrate is manufactured by Ballard Power Systems. The physical specifications of AvCarb^{TM} P50 are illustrated in Table 4-1. The process of making a carbon-fiber paper starts with carbonization at the temperature of 1200°C in an inert atmosphere followed by chopping the material and adding a binder (e.g. epoxy or wax) to form paper sheet. To achieve the desired thickness, impregnation of resin allows the material to be moulded to the correct thickness. Next the material is graphitized at temperature of 2000°C or above to add conductivity into the carbon-fiber sheet (Barbir, 2005). AvCarb^{TM} P50 is chosen as the 3-D extended anode electrode because it provides a perfect balance between mechanical integrity, effective diffusivity to liquid fuel together with good conductivity and porosity for distribution of catalyst particles.

Table 4-1: Physical specification of AvCarbTM P50 carbon fiber paper (http://www.fuelcellstore.com/en/pc/)

Material	AvCarb^{TM} P50 (Manufactured by Ballard Power Systems)
Thickness (μm)	172
Electrical resistivity (mΩ cm)	9.7
Bulk density	0.28
Tensile Strength (N m $^{-1}$)	1000
Thermal Conductivity (W m^{-1} K^{-1})	1.3 (at 100°C)
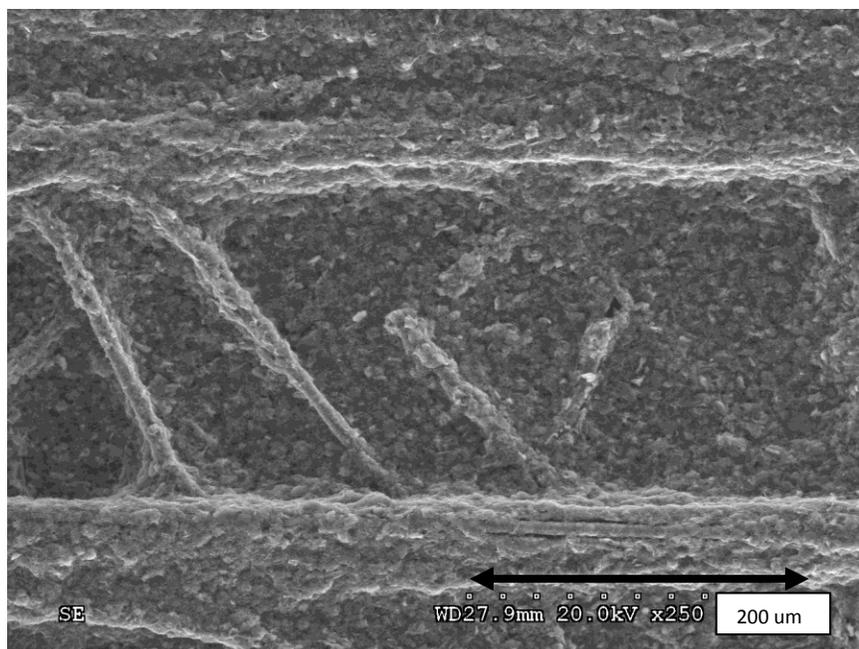
Figure 4-1:Uncatalyzed carbon fiber (AvCarbTM P50)

4.2 Substrate pre-treatment

The surface of the carbon fiber is not active enough to reduce the metal salt from the chemical bath solution, and thus needs to be activated prior to electroless deposition. The surface of carbon fiber can be modified by chemical and heat treatments to generate surface chemical functional groups at the surface. Different thermal and chemical treatment can selectively increase or remove the concentrations of surface functional groups such as oxygen, hydroxyl and carbonyl groups. To improve the substrate surface catalytic activity towards reductive reaction, two chemical treatment methods of tin/palladium solution and nitric acid wash were investigated.

4.2.1 Nitric acid treatment

Treatment of carbon fiber in 5 wt% nitric acid solution was a successful activation process and it was conducted separately from the Sn/Pd solution treatment (discussed in section 4.2.2). The nitric acid pre-treatment process is also applied to compare the degree of substrate activation with Shipley solution treatment.

The AvCarb[TM] P50 carbon fiber paper was cut into 5 cm^2 geometric area and immersed in 5 wt% nitric acid solution for 15 min. The temperature of 5 wt% nitric acid solution was kept constant at during the treatment. Afterward, the substrate was washed thoroughly with de-ionized water and dried at room temperature.

It is reported that the treatment of carbon surface with low concentration nitric acid solution (<10 wt%) produces significant number of oxygenated acidic surface groups onto the carbon surface when nitric acid solution is heated to 323 K (Li et al, 2005). One advantages of nitric acid chemical treatment is that it does not change the pore characteristics at the surface.

4.2.2 Shipley-type solution pre-treatment

Shipley-type solution was prepared fresh by mixing palladium chloride aqueous solution with stannous chloride and hydrochloric acid prior to pre-treatment of AvCarb[TM] P50 substrates. Shipley dispersion system produces a lyophilic colloid which can be accelerated with hydrochloric acid to provide a sensitizing layer for subsequent chemical deposition of Pd catalyst (Tran & Langer, 1993). Through the surface redox reactions between carbon, Pd^{2+} ,Sn^{2+} ions , all the Pd^{2+} spontaneously reduces to Pd as Sn^{2+} oxidizes to SnO_2 and Sn^{4+} . Some of the carbon oxidizes to –COH,-CO,-CHO,-COOH and CO_2 (Tran & Langer, 1993). The presence of metallic species such as Pd and SnO_2 on the surface of AvCarb[TM] P50 as the result of Shipley-type pre-treatment activates the substrate for Pd catalyst deposition (Cheng & Gyenge, 2009). The procedure follows the immersion of 5 cm^2 geometric area of carbon fibre in the Shipley-type solution (6 mM $PdCl_2$ + 0.3 M $SnCl_2$) at the temperature of 333 K for 30 min. Afterward, substrates were washed thoroughly with de-ionized water; air dried for 5 hours and kept in a clean environment.

4.3 Catalyst deposition

The deposition method employed in this study, is the electroless or chemical deposition. Upon activation of electrode surface with the aid of Shipley or nitric acid solution, the electroless deposition is employed to disperse Pd particles on the surface of the AvCarb[TM] P50 substrate. The steps and the chemical composition of the electroless bath are explained in following section.

4.3.1 Electroless deposition method

Electroless catalyst deposition refers to the chemical deposition of Pd from a Pd salt (e.g. $PdCl_2$) on the substrate (carbon fibre) in the absence of external electric source (Shu & Grandjean, 1993). Electroless deposition of Pd was carried out by contacting the activated substrate (AvCarb^{TM} P50) with an aqueous solution containing 0.1 M $PdCl_2$, 2 M of formaldehyde as the reducing agent and 0.002 M of saccharine for stabilizing the chemical bath (Table 5-1).

All chemicals were reagent grade and obtained from Sigma-Aldrich. To investigate the effect of Nafion® (perfluorinated resin solution, 5 wt%) on dispersion of Pd particles, different concentration of Nafion® between 1.27 , 2.46 , and 4.66 g/L were added to the solution before adding the reducing agent. The electroless deposition was carried out in a water-jacketed glass vessel connected to a circulating water bath at temperature of 333 K. The chemical bath constituents (excluding formaldehyde) were mixed completely for 15 min and reached temperature of 333 K,then the reducing agent (formaldehyde) was added to the solution.

The AvCarb^{TM} P50 substrate was immersed right after introducing the reducing agent. At 45 min when the chemical reduction of Pd ions is completed, the electrode was washed thoroughly with distilled water and air dried at room temperature. Three different substrate immersion times in the electroless bath were tested to assess the effect of longer exposure time on the dispersion of Pd catalysts. Also variable Nafion® concentrations were introduced separately at each different electrode immersion time to obtain the effective Nafion® concentration and exposure time. The range of Nafion® concentration (g/L) added in respect to electrode immersion time in deposition processes are shown in Table 4-2.

Table 4-2: Nafion® concentration and immersion time variable values

Electrode exposure time (min)	5 wt% Nafion® perfluorinated resin solution volume added to the chemical bath (ml/50 ml of electroless solution)
No Nafion® content	
45	0
15	0
5	0
1.27 g/L Nafion® content	
45	1.5
15	1.5
5	1.5
4.66 g/L Nafion® content	
45	6
15	6
5	6

4.4   Characterization of deposited catalyst particles

The surface characteristics and morphology of catalyzed substrates were evaluated by Scanning Electron Microscopy (SEM) at Material Engineering Department at University of British Columbia[1]. Also, to assess the loading of dispersed Pd and Sn particles on the substrate's surface ICP-AES analysis were conducted by Maxxam analytical[2].

4.4.1   Particle size by scanning electron microscopy (SEM)

High resolution Scanning Electron Microscopy (SEM) branded as Hitachi S4700 working with an accelerating voltage of 2000V and emission current of 1.25×10^7 A was used to observe the surface morphology. Electrodes were cut into 1 cm^2 pieces and mounted onto SEM stubs with carbon adhesive for analysis. The working distance of 0.0025-0.0035 m was employed for high resolution analysis.

---

[1] Electron Microscope Lab, Materials Engineering Department, UBC, 419 - 6350 Stores Road, Vancouver, B.C.
[2] Maxxam Analytics Lab, 8577 Commerce court, Burnaby, B.C.

4.4.2 Inductively coupled plasma atomic emission spectroscopy (ICP-AES) analysis

ICP-AES analysis was used to determine the loading mass of Pd and Sn particles on each substrate using a Perkin Elmer Optima, model 3300 DV instrument at Maxxam analytical laboratories. The PdSn/C samples were cut to fragments of 1 cm^2, weighted and dissolved in HCl-HNO$_3$ solution for three hours. The dissolved PdSn/C particles in solution then were diluted and analyzed by the ICP-AES method.

4.5 Half- cell electrochemical experiments

Half-cell electrochemical experiments were conducted with a three-electrode setup comprising of Hg/Hg$_2$SO$_4$, K$_2$SO$_4$ std, the reference electrode, and Pt wire as the counter electrode together with the working electrode. Electrodes with dispersed Pd and Sn particles were cut into 1 cm^2 pieces to be employed as working electrode. The water jacketed vessel was warmed and stabilized at 298 K with electrolyte solution of 1 M HCOOH and 0.5 M H$_2$SO$_4$. A potentiostat was provided by Radiometer analytical (operating on PGZ402 Voltalab software). All half-cell electrochemical experiments are measured against the mercury/mercurous sulphate (MSE) reference electrode. The main components of half-cell electrochemical cell including working electrode, reference electrode and auxiliary electrode are depicted in Figure 1-4.

4.5.1 Cyclic voltammetry

Cyclic voltammetry scans were conducted between -670 mV to 670 mV vs. MSE at the scan rate of 50 mV s^{-1} at 298 K. During the potential sweep, plots of current versus applied potential named as cyclic voltammograms were obtained. Prior to the actual cyclic voltammetry experiments, the catalyzed anodes were electrochemically cleaned in a 0.5 M H$_2$SO$_4$ solution at 298 K for 30 seconds to oxidize possible organic residues and also reducing the oxides on the surface of the anode. After substrate cleaning, actual cyclic voltammetry (CV) tests were carried out in an electrolyte solution of 1 M HCOOH and 0.5 M H$_2$SO$_4$ that was purged with nitrogen gas for 30 min prior to tests.

4.6   Fuel cell test

The fuel cell polarization experiments were performed to assess the performance of catalyzed anodes in a direct formic acid fuel cell. The fuel cell tests were conducted on different anodes that were prepared with variable Nafion® concentrations to compare the performance characteristics in regards to Pd mass loading and pre-treatment methods. The direct formic acid fuel cell was assembled with two gold-plated end plates, an Elat® carbon cloth from E-Teck Inc, prepared half-MEA that sealed with silicon-coated gasket. The serpentine flow field incorporated into end plates provides uniform fuel and gas distribution that is beneficial for thin anodes (~100 µm) (Bauer, Oloman, & Gyenge, 2009). The fuel cell test station was operated on the FC Power® software from Federis Inc. Fuel concentration of 1 M HCOOH and 0.5 M H_2SO_4 were mixed and prepared fresh prior to the test and fed to the test station at 3 cm^3 min^{-1} through a peristaltic pump .The oxygen flow rate of 500 standard mL min^{-1} to the fuel cell at 333 K and 2.5 bar (abs) was maintained. The fuel cell test system was allowed to stabilize for 2 hours to reach the operating temperature. This step is important to assure the stability and reproducibility of the system prior to current draw. The current was continuously drawn at intervals of 30 s and the resulting voltage was recorded at each current input. The fuel cell test assembly is shown in Figure 4-2 below.
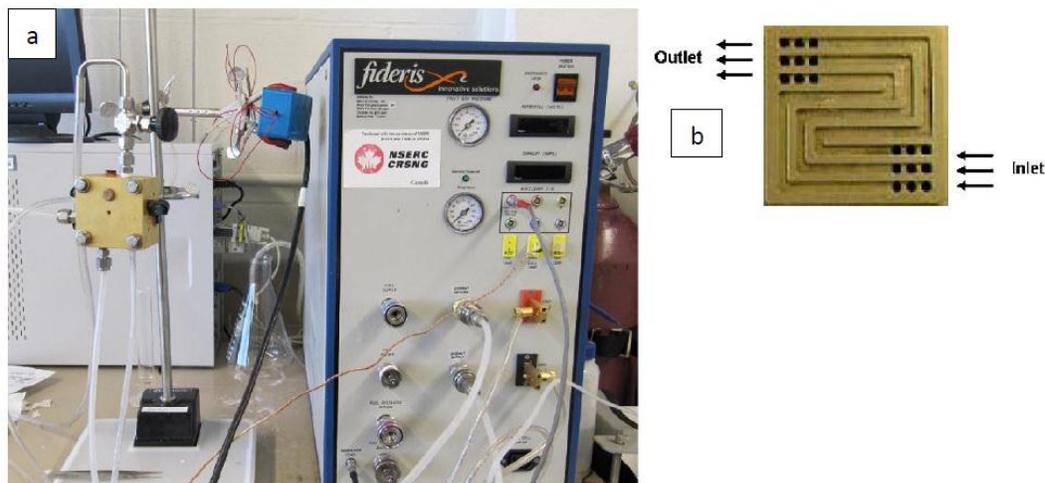
Figure 4-2:(a) fuel cell test station;(b) serpentine flowfield incorporated into end plate (as supplied by Fideris Inc).

4.6.1   Membrane electrode assembly (MEA) fabrication method

The cathode half membrane electrode assembly (MEA) was prepared by spraying catalyst ink solution containing Pt black particles. A Nafion® 117 membrane (Fideris Inc) was first cleaned with distilled water followed by conditioning in 5 wt% H_2O_2 at 343 K for 50 min. Next, the membrane was immersed in 0.5 M H_2SO_4 for 10 hours at 323 K to remove organic impurities. After cleaning the Nafion®117 membrane, it was cut into 5 cm^2 and loaded with 40 g m^{-2} of Pt catalyst by spraying the ink solution constantly with aid of computer numerical controlled (CNC) machine (Figure 4-3,a). The CNC machine used in this study is a motorized board that is movable relative to the sprayer attached on an arm. The sprayer is attached to the ink reservoir containing catalyst ink solution. A sample of coated Nafion®117 membrane prepared by CNC machine is shown in Figure 4-4,b.
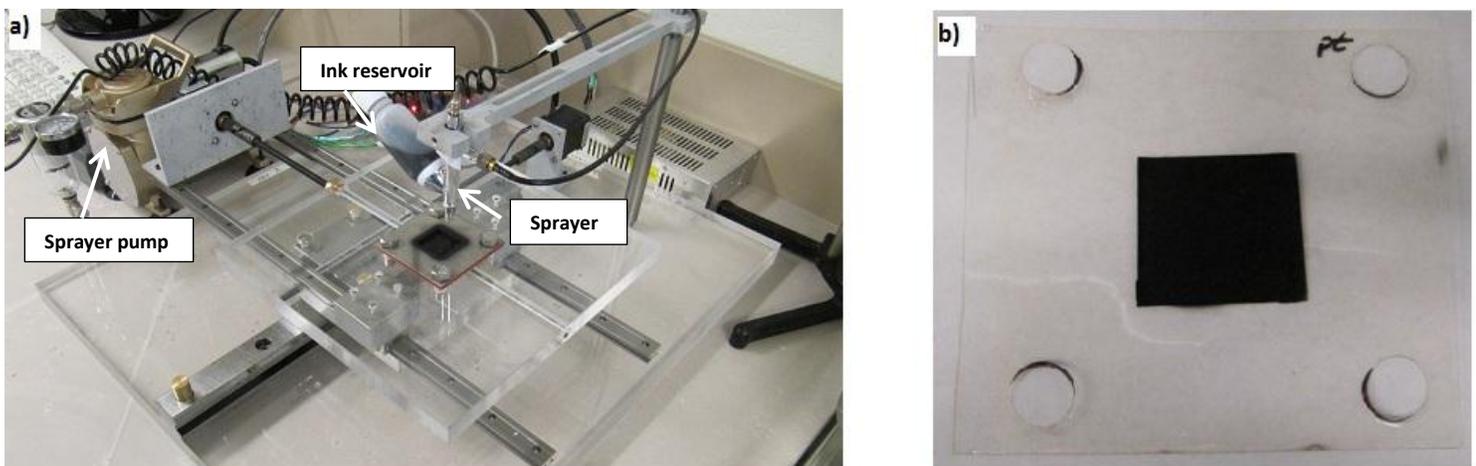
Figure 4-3:(a) CNC machine customized by Vincent Lam in 2009. (Chemical and Biological Engineering Department, UBC, Canada) ;(b) half-MEA prepared by spraying Pt catalyst ink on Nafion® 117 membrane.

5.0   Result and discussion

Electroless deposition experiments were carried out at 333 K to study the effect of altering Nafion® perfluorinated resin solution concentration and substrate immersion time on particle size, catalyst mass loading and catalytic activity. Exploratory deposition experiments indicated the positive effect of Nafion® solution, employed as an additive in the electroless bath, on the Pd surface morphology and mass loading. Also, the effects of substrate pre-treatment by nitric acid and Shipley-type ($PdCl_2$ + $SnCl_2$) solution were investigated. Figure 5-1 illustrated the experimental variables affecting the Pd deposition in the electroless bath.
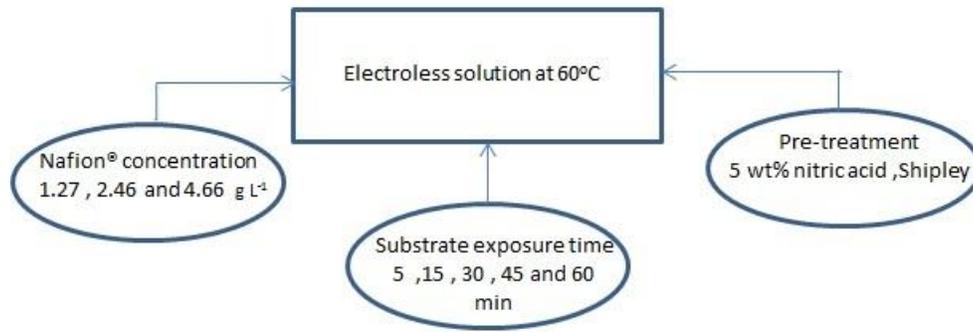
Figure 5-1: Electroless solution experimental variables

The three main experimental steps conducted to deposit Pd particles on carbon fiber paper were: 1- pre-treatment of substrate surface, 2- chemical (electroless) deposition and, 3- catalyzed substrate post-treatment. The effectiveness of Pd electroless deposition on the carbon fiber surface is tested by varying experimental conditions such as treatment time and additive concentration as explained in Section 4. The effects of experimental variables are analyzed in an order shown in Figure 5-2. Similar steps are followed in terms of Shipley type solution pre-treatment.

The aim was to assess the effect of each variable to obtain the most effective experimental condition resulting in an enhanced catalyst dispersed anode.

To make sure the electroless deposition method produces the same amount of particle mass loading, two repetitions are conducted on the electroless deposition and the average catalyst mass

loading is found .In this section, the impact of alternating electrode exposure time and Nafion® concentration are studied and discussed.
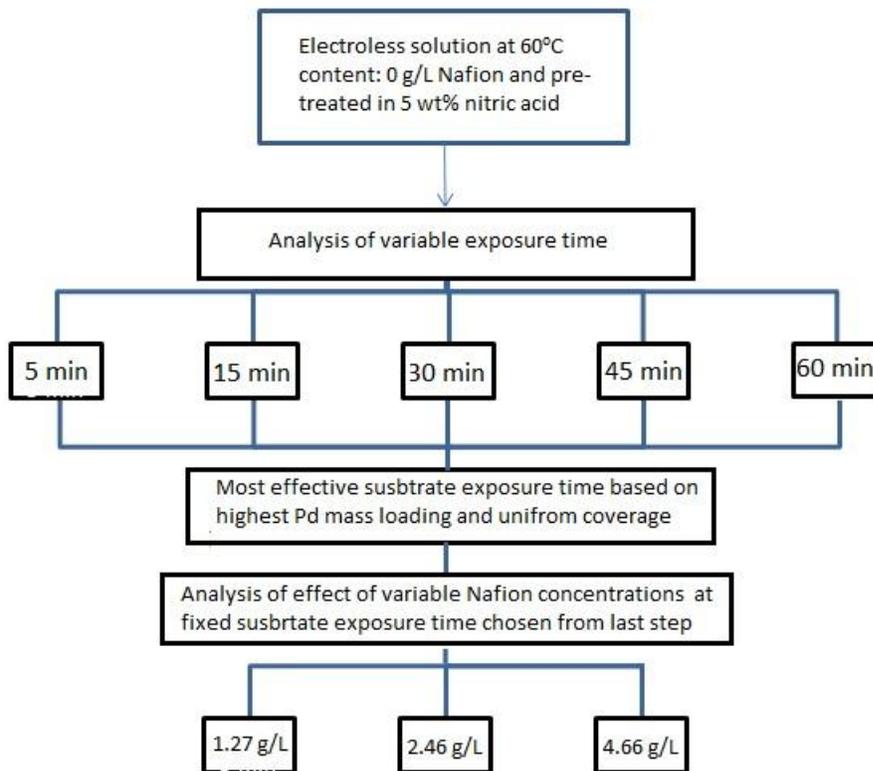
Figure 5-2: Flow chart of the electroless deposition experiment

5.1   Pre-treatment methods

There are various pre-treatment methods to activate and enhance the surface properties of carbon material prior to catalyst deposition. Two surface activation methods of acid treatment (5 wt% nitric acid solution) and Sn/Pd solution (known as Shipley-type solution) were investigated separately. Both methods sensitized and activated the substrates surface towards reduction of Pd particles from Pd salt ($PdCl_2$) in the electroless solution.

5.1.1 Nitric acid pre-treatment

It is known that the physicochemical and catalytic properties of carbon are linked to the various surface functional groups (e.g. oxygen containing and nitrogen containing groups) that exist on the porous surface of carbon material (Li et al, 2005). The degree of interaction between chemical bonding and metal particles can be enhanced by increasing the fiber active surface area sites (ASA) through acid treatments including nitric acid wash.

In order to investigate the effect of nitric acid treatment on catalyst loading, two AvCarb^{TM} P50 electrodes were tested in the electroless solution containing 1.27 g L^{-1} Nafion® with only one electrode pre-treated in nitric acid solution prior to deposition process at temperature of 323 K. The positive impact of the nitric acid pre-treatment on the carbon fiber surface activation is proven by obtaining larger Pd mass loading compared with the non-activated substrate (Figure 5-3). Deposition on the nitric acid pre-treated substrate yielded a mass loading of 4.6 mg cm^{-2} that is about 3 times increase in loading compared with un-activated substrate. The standard deviation of Pd mass loading was found to be 0.10 mg cm^{-2} for two replications of electroless deposition upon nitric acid pre-treatment. Factors such as the degree of nitric acid concentration and acidity of the treatment solution also affect the amount of oxygen-containing groups on the surface of carbon material (Li et al, 2005).

The pre-treatment with high concentrated nitric acid (above 45 wt%) could weaken structurally the carbon fiber and introduce a great amount of oxygenated functional groups that blocks the entrance of pores and also provides a strong interaction between oxygen-containing groups and Pd metal precursor that limits the Pd dispersion (Passalacqua & Lufrano, 2001).

Treatment in dilute nitric acid solution (5 wt%) was shown to be the most effective concentration in introducing the right amount of oxygenated acidic surface groups which is followed in this study (Li et al, 2005). The higher Pd loading achieved on nitric acid pre-treated substrate could be explained by the introduction of oxygenated functional groups that roughens the surface and improves the catalytic activity towards dispersion of Pd. Also, oxidation of porous carbon fiber surface enhances the acidic property and removes the mineral elements that might poisons reductive reactions.
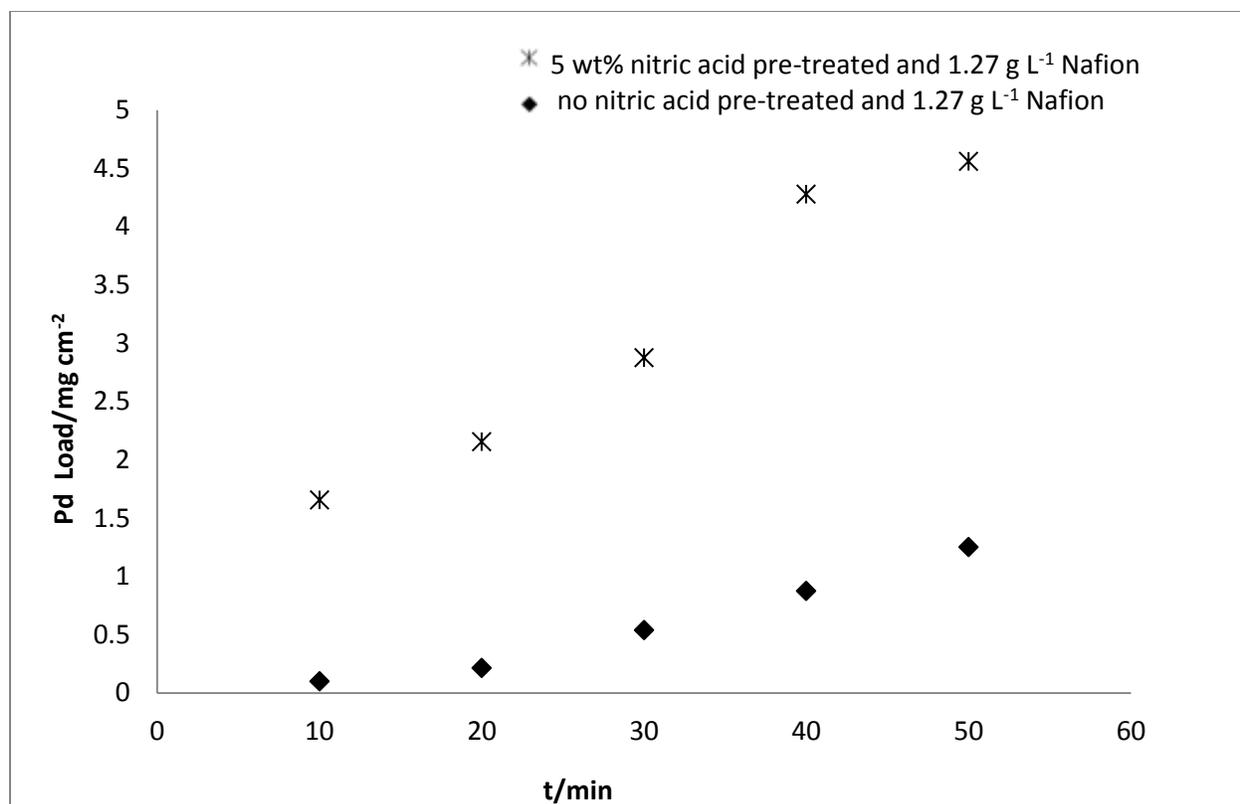
Figure 5-3: Effect of 5 wt% nitric acid pre-treatment on Pd mass loading (mg cm^{-2}) with varying electroless exposure time at fixed Nafion® concentration of 1.27 g L^{-1} in the chemical bath at 333 K.

5.1.2   Shipley solution pre-treatment

The Shipley-type solution (6 mM P$_2$dC1 and 0.3 M SnC1$_2$ in 4 M HC1) also activates the carbon fiber surface and enhances the surface characteristics for subsequent electroless Pd deposition similar to nitric acid wash. A comparative analysis between electrodes catalyst loading sensitized by Shipley solution and un-activated electrode proved the positive effect of Shipley treatment.

Figure 5-4 shows the SEM pattern of Pd catalyst supported on the carbon fiber substrates with Nafion® content of 4.66 g L^{-1} for treated and untreated samples in Shipley solution. The Pd deposition rate on the carbon fiber support increased dramatically being completed in less than 20 min (in contrast to 50 min on untreated support), reflecting the higher activity of Shipley treated substrates. The substrates pre-treated in Shipley solution for 30 min resulted in a fairly dense coating with Pd-Sn agglomerates of diameter ranging from 0.40-0.55

µm (Figure 5-4, C) and uniform layer of Pd particles at the electrode surface. The Pd and Sn mass load, Pd:Sn atomic ratio and their respective Nafion® concentration are shown in Table 5-1.

Table 5- 1: Variable Nafion® solution concentrations (0, 1.27 and 4.66 g L^{-1}) and Pd, Sn content on AvCarbTM P50 when pre-treated in Shipley-type solution.

Nafion® concentration g L^{-1}	Pd (mg cm^{-2})	Sn (mg cm^{-2})	Pd:Sn
0	0.0057	0.0244	1:3.8
1.27	1.33	0.0163	90:1
4.66	1.64	0.0746	24:1

The presence of 4 M HCl accelerator in Shipley-type solution dissolves the protective layer and therefore greater surface area for the catalytic Pd-Sn nuclei is exposed (Tran & Langer, 1993). When the activated carbon fiber substrates are immersed in the electroless solution, Pd metal deposition occurs at these catalytic sites. The experimental analysis on the effect of pre-treatment time show that longer treatment time in Shipley solution does not favour the deposition of Pd particles. In fact, all samples treated for 60 min showed lower Pd mass loading compared to 30 min treated substrates.

The effectiveness of Shipley-type solution for promoting adherence of Pd particles to carbon surface was also proven for graphite felt substrates in fabrication of formic acid fuel cell anode catalyst electrodes (Cheng & Gyenge, 2008).
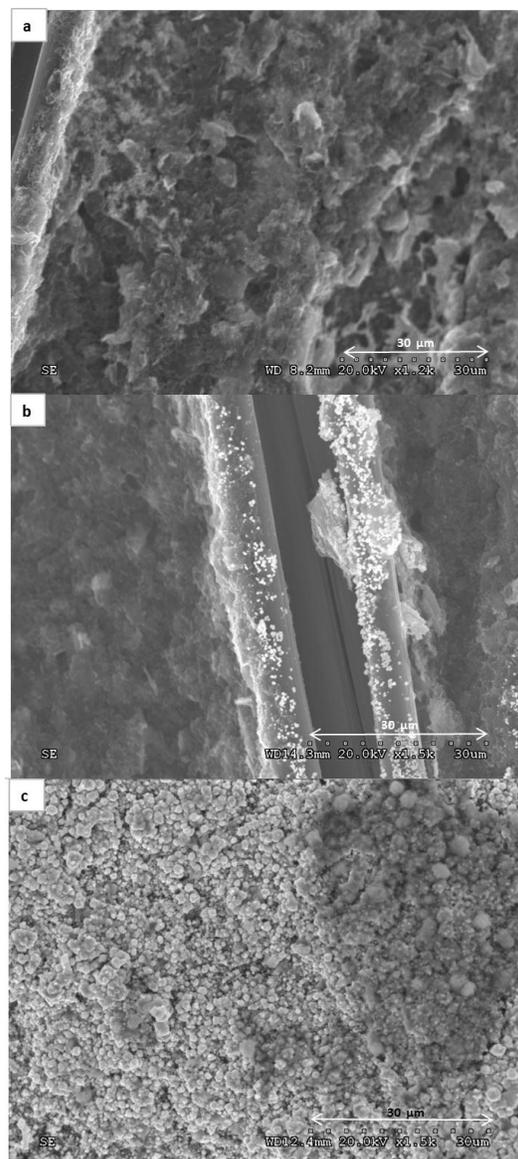
Figure 5-4: SEM images of (a) naked substrate;(b) deposited Pd/C substrate with no Shipley pre-treatment and Nafion content (4.66 g L^{-1});(c) Shipley treated Pd/C substrate and Nafion® content of 4.66 g L^{-1} at 333 K and 45 min.

The three way relationship between Pd mass load, Nafion® concentration and treatment time in Shipley-type solution is depicted in Figure 5-5. In terms of the Pd mass loading, the effective concentration of Nafion® is achieved at 4.66 g L^{-1} when pre-treated for 30 min in Shipley-solution. The positive interaction effect between Nafion® and Shipley pre-treatment for 30 min in Pd dispersion is evident in Figure 5-5.

The enhanced Pd mass loading can be explained by the presence of higher tin content (formation of SnO_2) on the surface that provides a stabilizing layer upon employing the Shipley pre-treatment and increase the number of nucleation sites formed from surface roughening (Langer & Tri, 1993).

Since the hydrophilic formic acid cannot penetrate within the anode diffusion media, the wettability characteristics of the carbon fiber surface are also important and are to be altered. Shipley solution affects the wetting properties of carbon fiber and makes it hydrophilic. As a result, Shipley pre-treatment could favour both the successful Pd dispersion and formic acid penetration (Cohen & Mekk, 1976).

The effect of Nafion® and Shipley-type solution on the catalytic activity of carbon supported Pd catalyst for formic acid oxidation was also investigated by electrochemical half-cell experiments. The cyclic voltammograms shown in Figure 5-6 are conducted on 0 , 1.27 and 4.66 g L^{-1} Nafion® electrodes in 1M formic acid + 0.5 M H_2SO_4 solution.
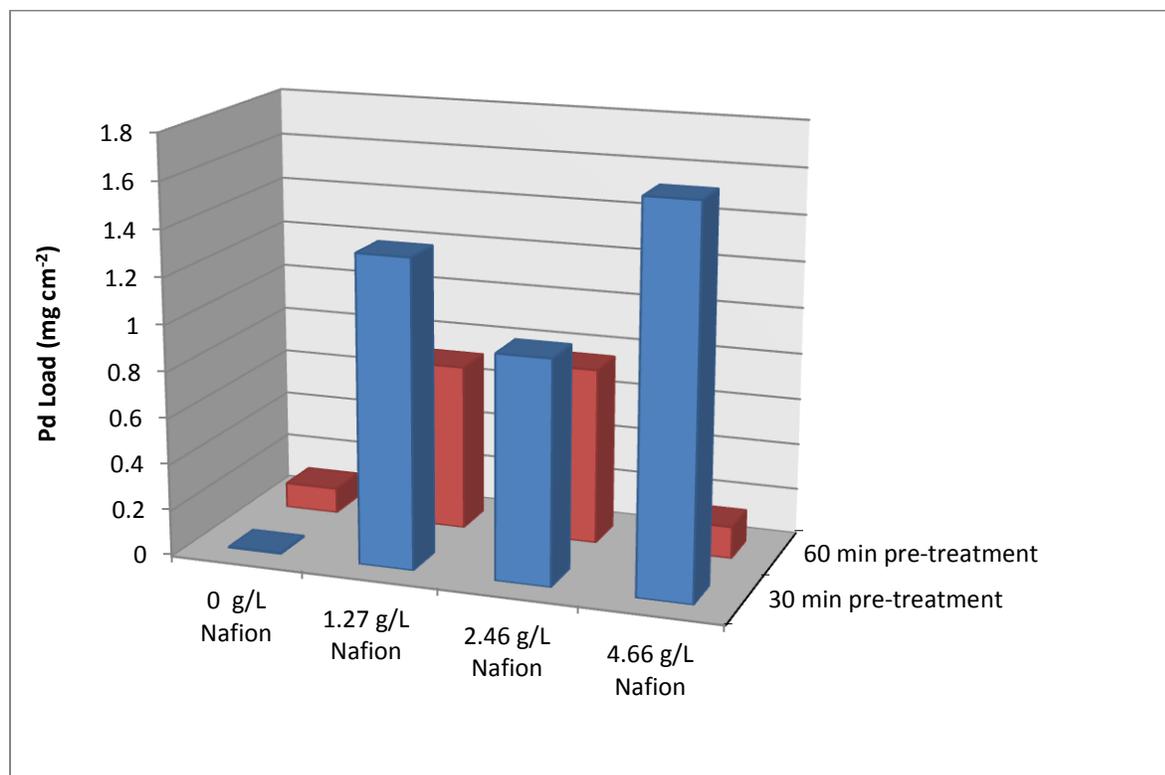
Figure 5-5: Pd mass loadings on AvCarbTM P50 with respect to Nafion® concentration and Shipley solution pre-treatment time.

5.1.3 Effect of deposition time on catalyst load

All carbon fiber substrates discussed in this section are pre-treated in 5 wt% nitric acid solution at 323 K for a period of 15 min prior to chemical deposition. To assess the effect of deposition time, three pre-treated carbon fiber substrates were catalyzed chemically at different treatment times, starting from 5 min to 45 min at fixed Nafion® concentration of 1.27 g/L. Afterward catalyzed substrates were rinsed with de-ionized water and air dried prior to surface analysis tests as described in Section 4. The temperature of the electroless bath was kept constant at 333 K by connecting the cell to a constant temperature control bath. The effective temperature range for electroless deposition of Pd was found within 40 to 353 K according to a study done by Kojima, et al. Commonly the rate of Pd plating increases as the temperature increases (Kojima & Hideto, 2010).

The chemical composition of electroless bath is presented in Table 5-2. Formaldehyde is the main reducing agent with 2M concentration. The reduction of Pd in the presence of formic acid and formaldehyde in the electroless bath is shown through Equation 5-1 to 5-3.

$$Pd^{2+} + 2e^- \leftrightarrow Pd \qquad\qquad E^o_{e,Pd^{2+}/Pd} = 0.915\ V \ \text{ vs. SHE} \quad \text{[Eq. 5-1]}$$

$$HCOOH + 2H^+ + 2e^- \leftrightarrow HCHO + H_2 \qquad E^o_{e,HCOOH/CH_2O} = 0.035\ \text{V vs. SHE} \quad \text{[Eq. 5-2]}$$

$$Pd^{2+} + HCHO + H_2O \leftrightarrow HCOOH + 2H^+ + Pd \qquad E^o_{Cell} = 0.88\ \text{V} \qquad \text{[Eq. 5-3]}$$
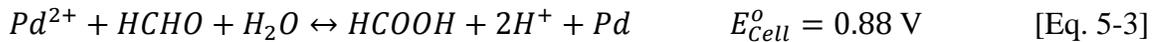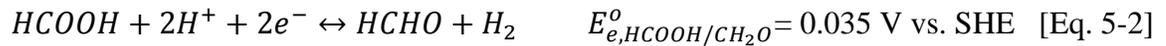
Also, the presence of an additive such as saccharin is common as a brightening agent (Glenn, Mallory , & Juan, 1990). Glenn and co-workers found that the complete reduction reaction of Pd species in the solution is beyond 20 min. The organic ligand in the electroless solution stabilizes the electroless solution by complexing with Pd ion to enhance the uniformity and adherence of Pd to the surface. The deposited substrate was found to be bright by naked eye, indicating that saccharine acts as the brightening agent.

Table 5- 2: Chemical composition of Pd deposition electroless bath (Glenn et al, 1990)

Electroless chemical bath constituent Temperature = 333 K	
Nitric acid	0.1 M
Formic Acid	0.4 M
Palladium Chloride	0.1 M
Formaldehyde	2 M
Saccharine	0.002 M

High resolution micrographs of three samples are presented in Figure 5-6. Both particle dispersion characteristics and loading mass are dependent on exposure time. Electroless deposition for 5 min yielded scattered coating composed of 0.45-0.50 μm particles with a few larger aggregates (Figure 5-6, a).

Larger clusters appeared to be rare and were found at random locations on the carbon fiber surface treated for 15 min (Figure 5-6, b). Increasing the exposure time to 45 min improves the surface morphology towards a more uniform network with rough surfaces and Pd clusters (Figure 5-6, c).

At 45 min deposition time, a complete surface coverage with dense particulate-like structure is achieved (Figure 5-6, c). However, there are still random open pores due to existence of larger channels in the original AvCarb[TM] P50 carbon fiber surface structure.

ICP-AES analysis on three samples revealed improved Pd mass loading with respect to exposure time at 0 Nafion® content is shown in Table 5-3 with standard deviations of 0.26 mg cm^{-2} for two replications. Catalyzed substrates were cleaned by successive dipping in de-ionized water and air dried for subsequent fuel cell tests.

Table 5- 3: Effect of electroless deposition time on Pd catalyst mass loading

Exposure time (min)	Pd mass loading (mg cm^{-2})
5	1.14
15	2.32
30	2.58
45	2.84
60	2.75

The Pd mass loading increased with longer immersion time of substrate in the electroless bath up to 45 min of exposure. Whereas, increasing the deposition time beyond 45 min does not necessarily raised the mass loading as it is believed reduction of Pd ions has been completed in about 45 min.

Successful deposition of Pd is also dependent on activation of carbon substrate in 5 wt% nitric acid solution prior to deposition step .The effects of nitric acid treatment is discussed in Section 5.1.1.
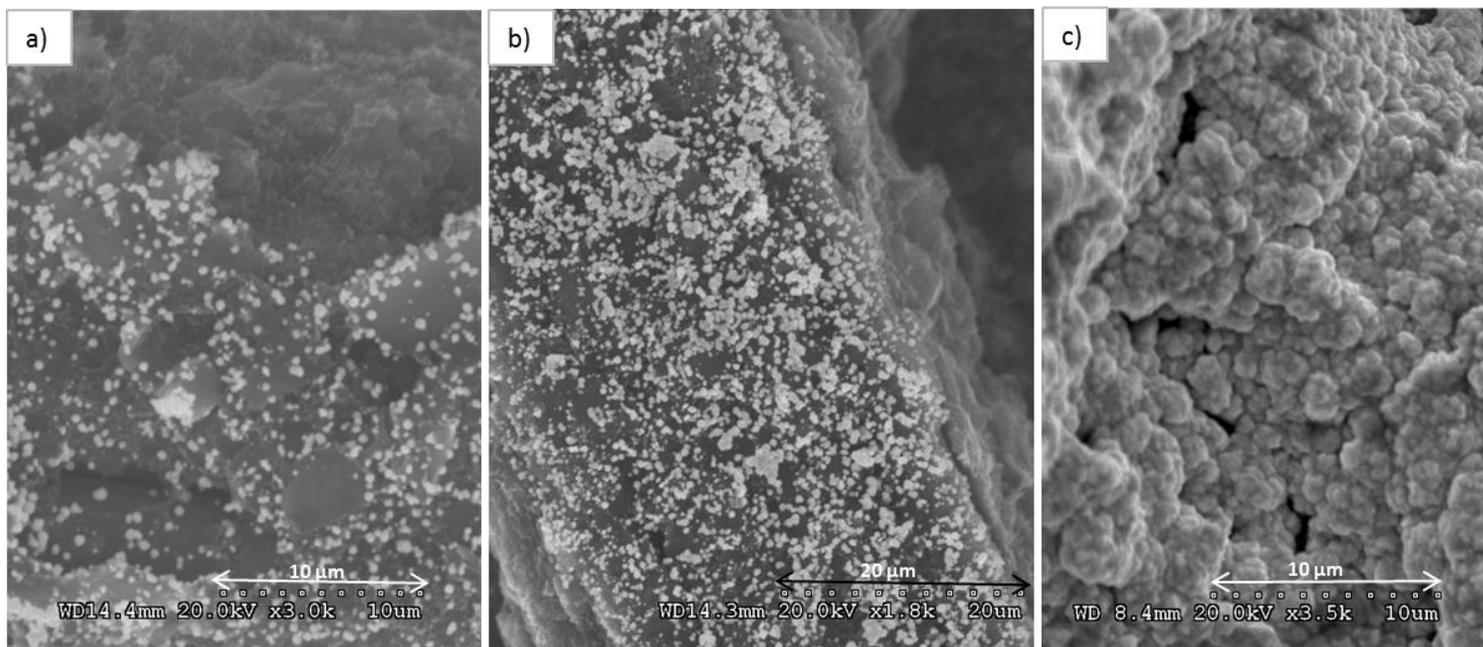
Figure 5-6: SEM images of electroless deposited Pd/C with nitric acid pre-treatment and fixed 1.27 g L^{-1} Nafion® and temperature of 333 K;(a) Substrate immersed for 5 min;(b) substrate immersed for 15 min ;(c) substrate immersed for 45 min in the chemical bath.

5.1.4   Effect of nafion® concentration

In the previous section, it was found that the substrate pre-treatment with 5 wt% nitric acid solution and longer immersion time up to 45 min in chemical bath enhanced the surface morphology and catalyst mass loading. Next, the effect of incorporating various Nafion® concentrations within the anode catalyst layer on carbon fiber surface is investigated. Pd particle deposition was carried out in the electroless solution at 333 K with addition of Nafion® at three different volume contents in the solution (0, 1.27 and 4.66 g L^{-1}) in separate deposition experiments for 45 min.

High resolution SEM images showed that incorporating higher Nafion® concentration within the catalyst layer produce a denser particulate-like structure due to large Nafion® aggregate formation (Figure 5-7) whereas at 0 g L^{-1} of Nafion® the surface shows naked AvCarb^{TM} P50 surface characteristics. The Pd mass loading of catalyzed substrate affected by

Nafion® solution are also shown in Table 5-4 indicating the gradual increase of loading corresponding to Nafion® concentration increase.

Integration of Nafion® solution into the deposition process connects the catalyst Pd particles (acting as electron conductor) to the Nafion® ionomer (acting as proton conductor) resulting in better catalyst utilization (McGoverna et al, 2003).

Table 5- 4: Pd catalyst mass loading on substrate pre-treated in 5 wt% nitric acid solution in presence of variable Nafion® content (standard deviations of +/- 0.1 mg cm^{-2})

Nafion® concentration (g L^{-1})	Treatment time (min)	Pd load (mg cm^{-2})
0	5	0.20
0	15	0.35
0	45	0.60
1.27	5	0.68
1.27	15	1.55
1.27	45	4.52
2.46	5	1.14
2.46	15	1.42
2.46	45	2.14
4.66	5	0.38
4.66	15	0.47
4.66	45	0.78

The obvious negative effect of Nafion® content at concentration of 4.66 g L^{-1} (Figure 5-7, a) is due to blockage of the catalyst sites and electrode pores when introducing high Nafion® concentrations. Whereas, the Nafion® content of 1.27 g L^{-1} results in notable difference in Pd dispersion and provides less bulky deposition characteristics. With 1.27 g L^{-1} Nafion® in electroless bath, a more uniform coverage (average particle size of 0.45 µm) with regular shape is observed.
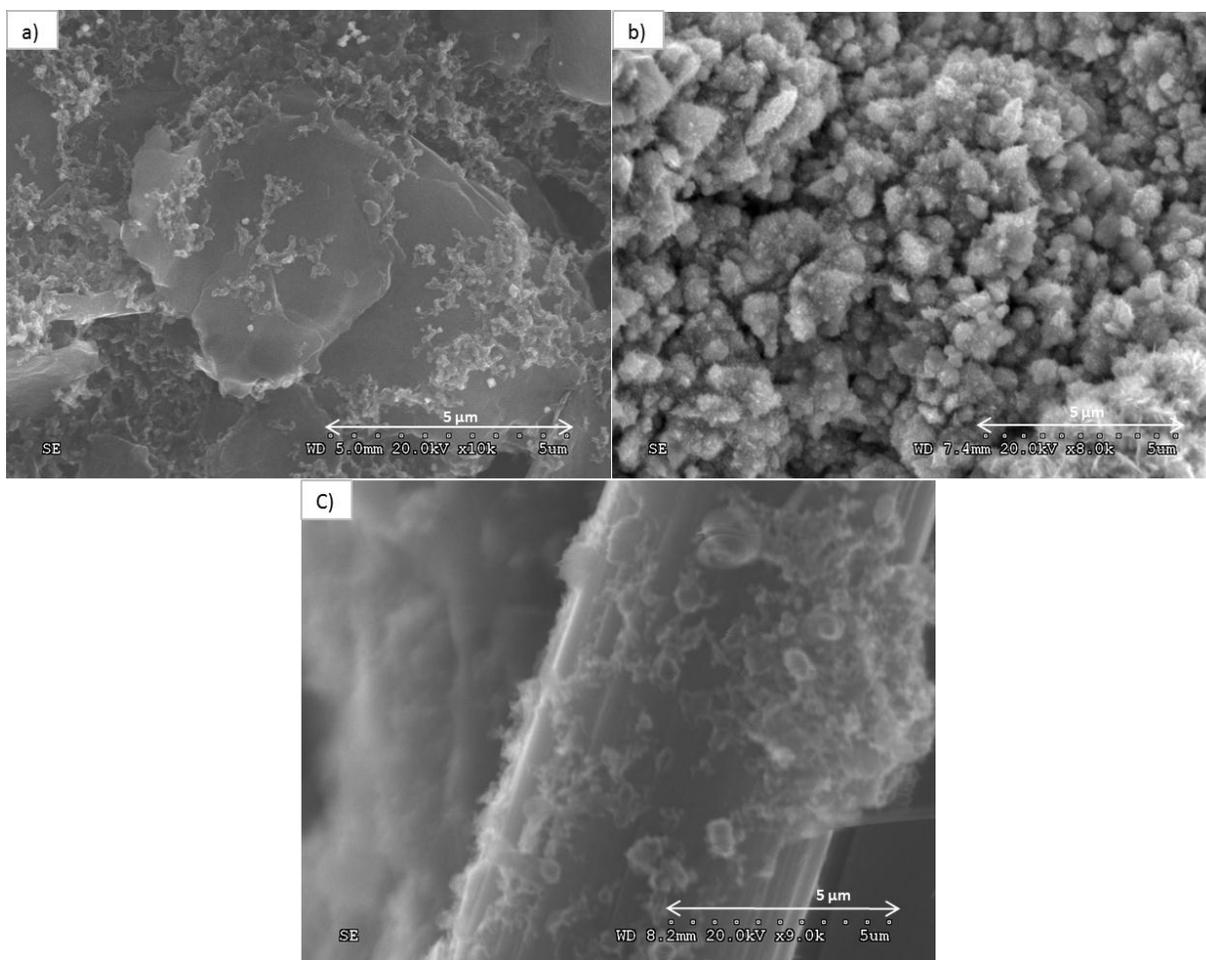
Figure 5-7:SEM images of electroless deposited Pd/C with 0 g L^{-1}, 1.27 g L^{-1} and 4.66 g L^{-1} Nafion® perfluorinated resin solution (5 wt%) at 333 K;(a) 4.66 g L^{-1} Nafion® solution in electroless bath and 15 min nitric acid pre-treatment ;(b) 45 min immersion with 1.27 g L^{-1} Nafion® solution and nitric acid pre-treated;(c) 45 min immersion with 0 g L^{-1} Nafion solution and nitric acid pre-treated.

Additional high resolution micrographs comparing the 1.27 g L^{-1} and 2.46 g L^{-1} Nafion® concentration in the electroless deposition solution indicated the presence of larger Nafion® agglomerates in the case of 1.27 g L^{-1} solution (Figure 5-7, b) with better Pd particle connection by Nafion® ionomer , compact and uniform distribution.

The optimum Nafion® concentration to achieve the effective Nafion® ionomer agglomerate size was found to be 1.27 g L^{-1} . According to a study done by Kanga et al., heat-treatment of Nafion® solution at temperature of 343 K in preparation of anode catalyst, monodispered the Nafion® ionomers and broke the Nafion® aggregates into smaller particles.

The temperature of the electroless solution bath in the current study was kept constant at 333 K which brings in the positive effect of heat treatment proven by Kanga study (Kanga et al, 2010).

Further analysis on the catalytic activity and effect of Nafion® ionomer in anode catalyst electrode design is discussed under cyclic voltammetry and the fuel cell performance in Section 5.1.5.
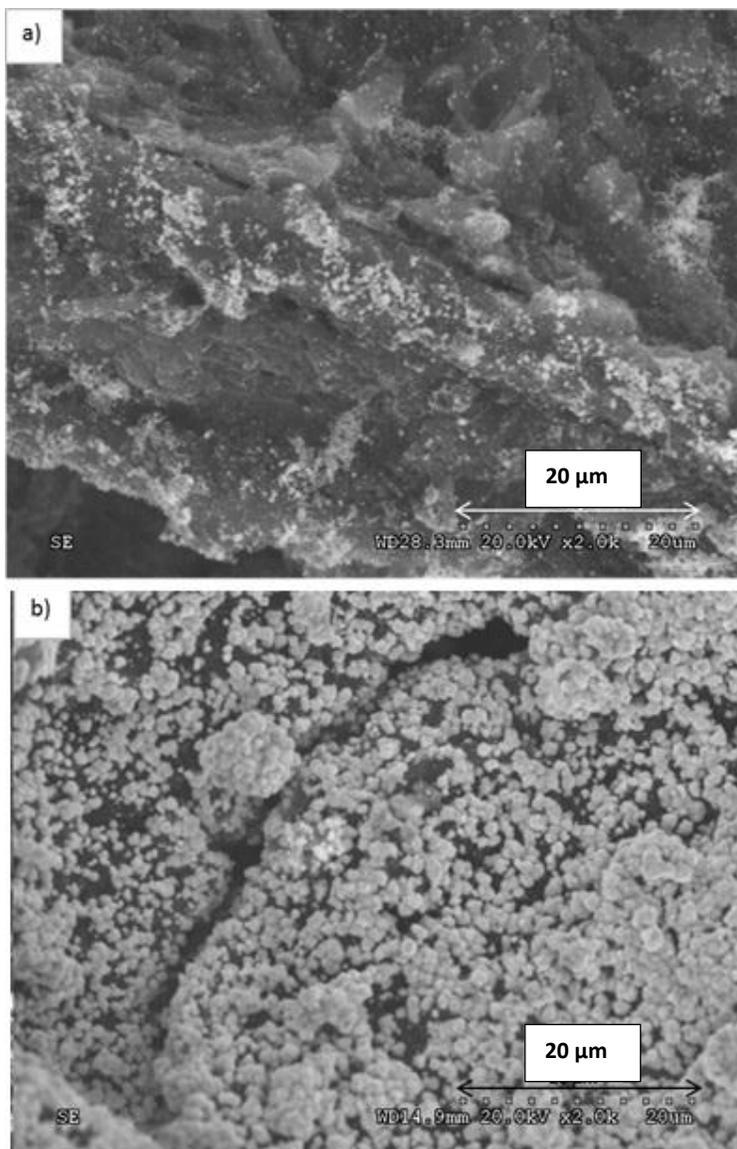
Figure 5-8:High resolution micrographs of deposited Pd/C .(a) 2.46 g L^{-1} Nafion® solution in electroless bath,15 min nitric acid pre-treatment ;(b) 1.27 g L^{-1} Nafion® solution, 15 min nitric acid pre-treatment at 333 K.

It is evident that, increasing the exposure time of substrate in the chemical bath above 20 minutes resulted in threefold increase in Pd mass load in the case of 1.27 g L^{-1} Nafion® incorporated substrate. The Pd mass loading follows a small gradual increase in the case of 4.66 g L^{-1} Nafion® treated substrate indicating a fairly naked surface as shown in Figure 5-8,a. The largest Pd mass load of 4.5 mg cm^{-2} corresponds to the substrate with 1.27 g L^{-1} Nafion® and deposition period of 45 min at 333 K.

5.1.5 Half-cell experiments

The observations discussed above based on SEM and ICP-AES analysis were in agreement with cyclic voltammetry studies shown in Figure 5-9. The superior kinetics of Pd/C electrode treated with 4.66 g L^{-1} Nafion® and Shipley solution compared with lower Nafion® affected electrodes is notable in Figure 5-9. Comparison with 0 and 1.27 g L^{-1} electrodes shows the peak current density of 500 A m^{-2} for 4.66 g L^{-1} Nafion® assisted electrode at the formic acid oxidation onset potential of -0.55 V vs. MSE.

On reversing the potential scan, the electrode surface remains inactive until the reduction of adsorbed intermediates on cathodic peak near 0.1 V vs. MSE is observed. The occurrence of this cathodic peak is most likely due to the oxidation of formic acid after reduction of surface oxides.
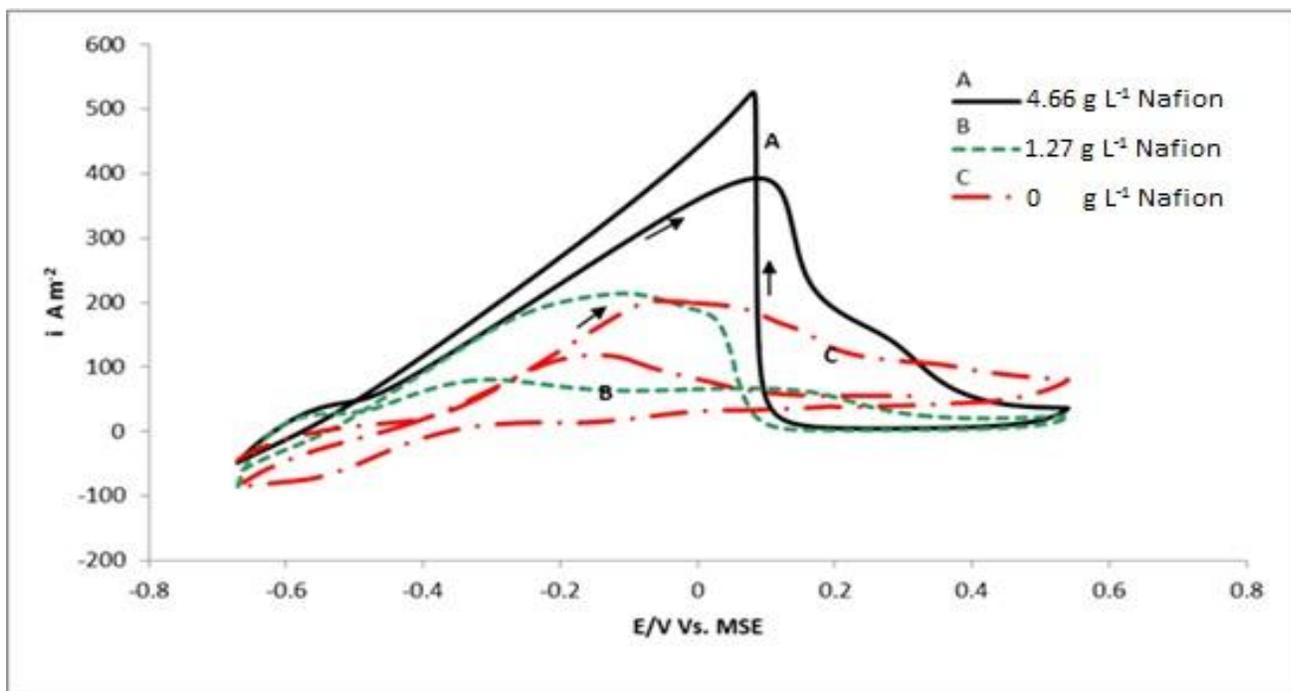
Figure 5-9:Three cyclic voltammograms of formic acid electro-oxidation in 1 M HCOOH and 0.5 M H$_2$SO$_4$. (A) 4.66 g L^{-1} Nafion® and 30 min pre-treatment by Shipley-type solution ;(B) 1.27 g L^{-1} Nafion® and 30 min pre-treatment in Shipley solution ;(C) no Nafion® and 30 min pre-treatment in Shipley solution. Temperature: 298 K; scan rate 50 mV s^{-1}.

The characteristics shape of cyclic voltammograms for different Nafion® incorporated samples were essentially similar to a study done by Cheng & Gyenge., on graphite felt supported Pd catalyst shown in Figure 5-10 (Cheng & Gyenge, 2009). Similar anodic/cathodic sweeps behaviour was shown by Liu et al., for Pd/C (Figure 5-11, A) that signify the formic acid oxidation via the non-CO$_{ads}$ intermediates pathway.
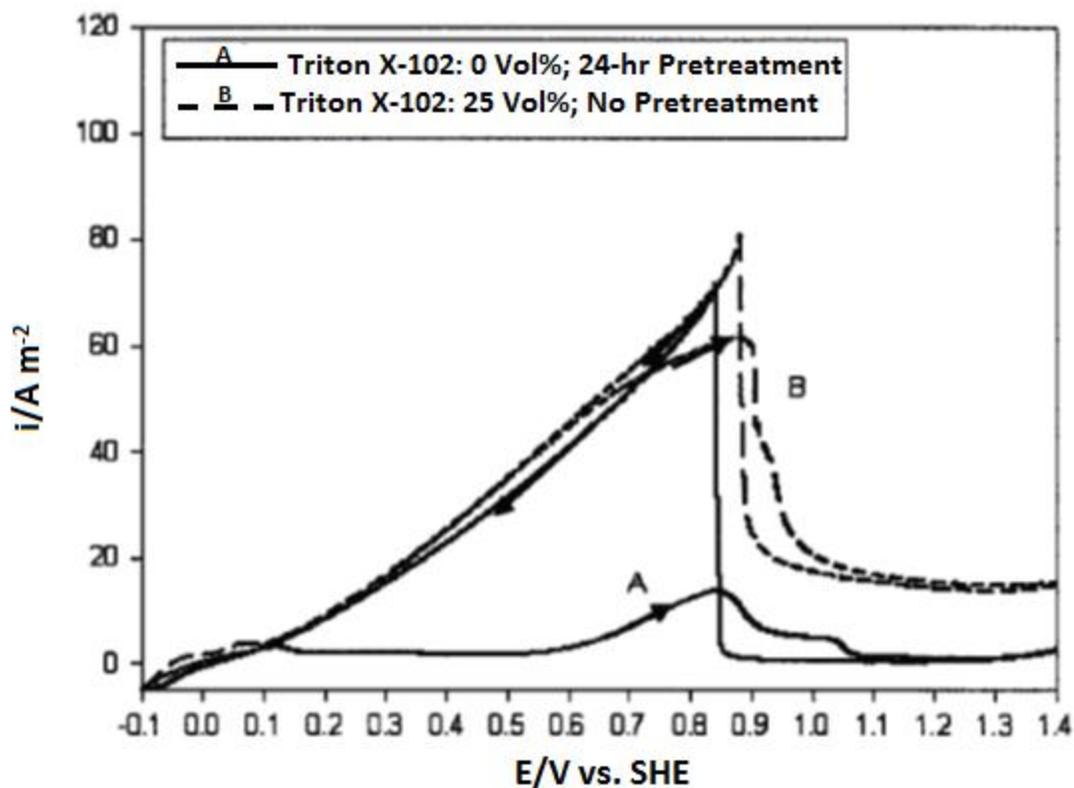
Figure 5-10: Cyclic voltammograms of formic acid electro-oxidation using Pd catalyst on graphite felt electrodes pre-treated by Shipley solution and surfactants affected in 1 M HCOOH + 0.5 M H$_2$SO$_4$ at 298 K (Cheng & Gyenge, 2009)

For Pd/C to take the non-CO$_{ads}$ pathway, the anodic and cathodic peaks are approximately close in terms of height and shape (Figure 5-11, B). This implies that same proportion of surface is available for reactions in anodic and cathodic sweeps and no blockage of active sites by CO$_{ads}$ intermediates occurs which confirm Equation 1-4.
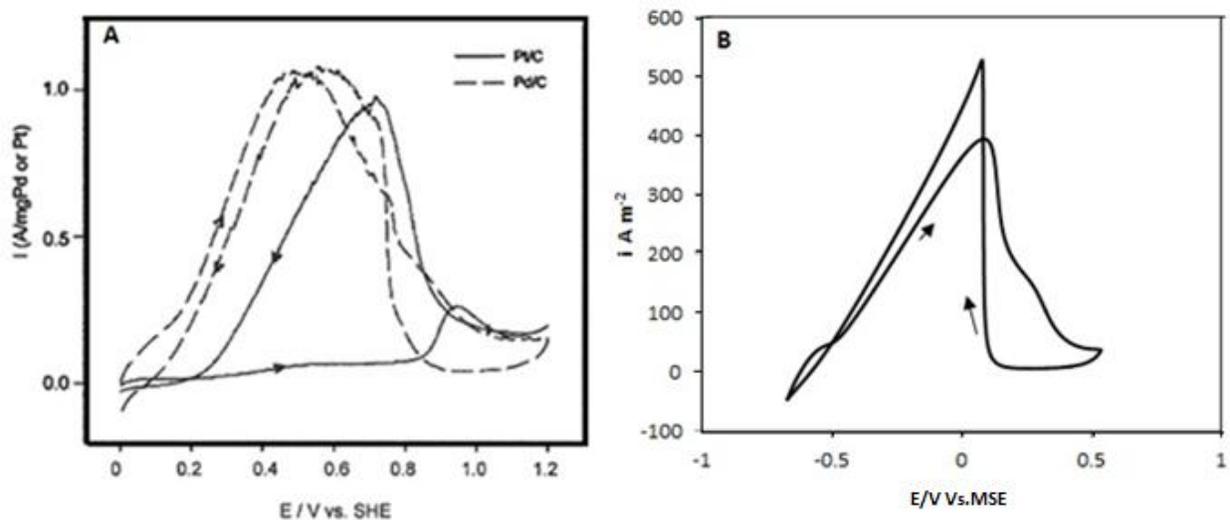
Figure 5-11: (A) Cyclic voltammogram of formic acid electro-oxidation with Pt/C and Pd/C. 3 M HCOOH and 1 M H$_2$SO$_4$ at 298 K. (Liu & Liang, 2006); (B) 4.66 g L^{-1} Nafion® assisted PdSn/C electrode, 1 M HCOOH and 0.5 M H$_2$SO$_4$ at 298 K.

Chronoamperometry experiments were conducted to assess the catalytic activity and long-term stability of formic acid electro-oxidation on PdSn/C electrode (Figure 5-12). The PdSn/C electrode with 4.66 g L^{-1} Nafion® indicated the highest initial catalytic activity that drops by 45% over 1 h of continuous operation at 0.65 V vs. MSE. The pattern of current decay was similar for each substrate. For the PdSn/C catalyst at 4.66 g L^{-1} Nafion® with highest Sn content, the current decay was slower than PdSn/C catalyst with lower content of Sn, supposedly because of less catalyst poisoning (Figure 5-12, C).

On the other hand samples employed with 0 and 1.27 g L^{-1} Nafion® content demonstrated a much lower initial current that approaches 0 after 1 h of operation. This rate of deactivation is in agreement with literature publication studies suggesting the presence of intermediate (e.g., COOH$_{ads}$) adsorption reaction. At potentials of 0.65 V vs. MSE the 4.66 g L^{-1} affected electrode delivered a current density that is 4 times larger than that of 0 g L^{-1} Nafion® affected electrode (Figure 5-12 A and C). Research done by Cheng & Gyenge., on surfactant assisted Pd/GF electrode also resulted in a total drops of 79% of initial oxidation current density after 3 hours at the potential of 0.65 V (Cheng & Gyenge, 2009).
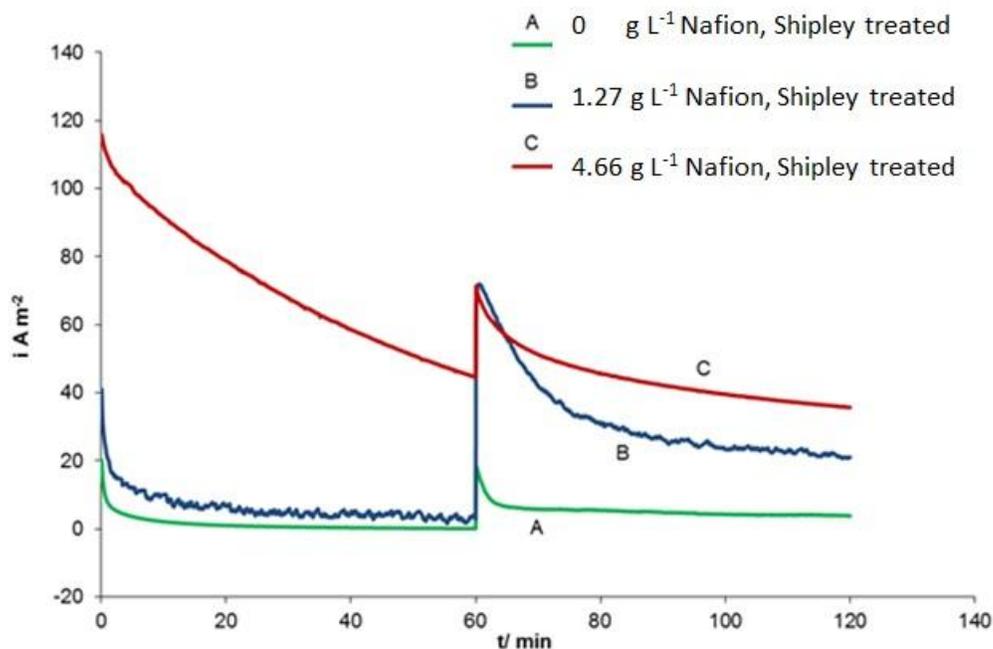
Figure 5-12: Chronoamperometry of formic acid electro-oxidation using Pd electroless deposited on carbon fiber (AvCarbTM P50). Electrolyte: 3 M HCOOH and 0.5 M H$_2$SO$_4$. Temperature: 298 K. (potential step applied at E1=-400 mV and E2=-200 mV).

5.2 Fuel cell tests

In order to understand the fuel cell system performance dependence on Nafion® concentration and surface activation methods, catalyzed carbon fiber substrates were evaluated by DFAFC tests. The polarization curves from the direct formic acid fuel cell test indicate the steady state open circuit voltage (OCV) of 0.70 V associated with the 4.66 g L^{-1} Nafion® assisted sample at 333 K (Figure 5-13). The corresponding OCV of 0 g L^{-1} Nafion® electrode was only 0.42 V that drops at the rate close to 4.66 g L^{-1} Nafion® incorporated sample. In Figure 5-13, the 1.27 g L^{-1} electrode outperformed the other electrodes and voltage decayed at the lower rate from 0.67 V of OCV. It is evident that the performance of DFAFC does not increase significantly passing from 1.27 g L^{-1}Nafion® to 4.66 g L^{-1} Nafion® .Correspondingly, the catalyst utilization decreases when the Pd loading is increases from 1.33 to 1.63 mg cm^{-2}. The sharper voltage drop in 4.66 g L^{-1} Nafion® assisted electrode could be explained by smaller

58

catalyst site availability for formic acid oxidation. That is reactant that could not reach the catalyst sites because they are blocked by Nafion® agglomerates.

It is clear on a metal loading basis (1.33 mg.cm^{-2}) the 1.27 g L^{-1} Nafion® assisted electrode provides the best system performance with the maximum power density of 16.8 W g^{-1} (Figure 5-15).
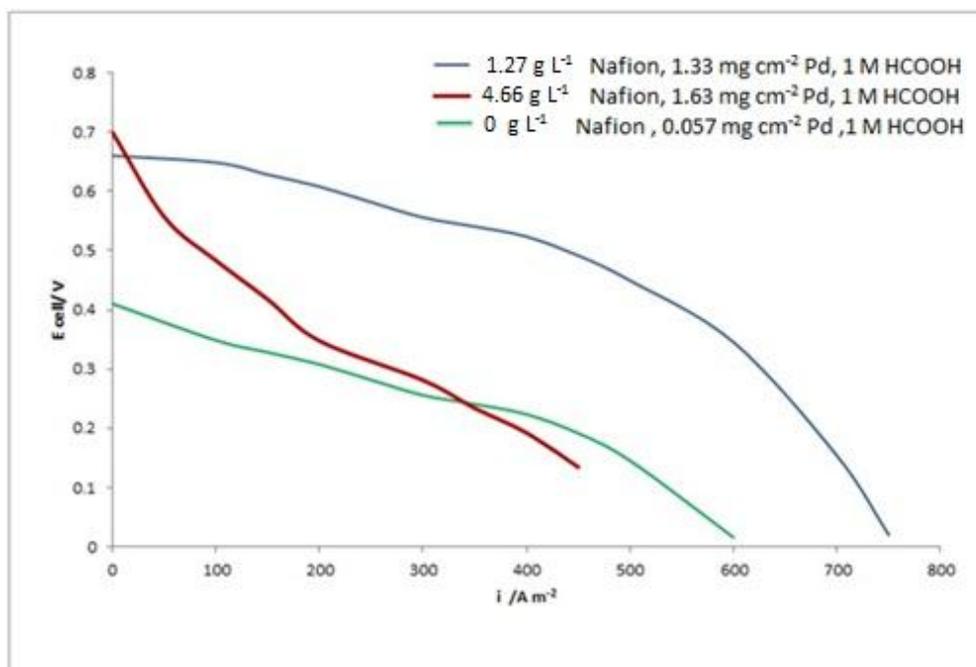
Figure 5-13: DFAFC polarization curve at 333 K-effect of Shipley-type solution treatment. The PdSn/C anodes were prepared with 0 to 4.66 g L^{-1} Nafion®. Fuel feed: 1 M HCOOH with 0.5 M H$_2$SO$_4$ and 3 ml min^{-1}; Cathode feed: dry O$_2$, flow rate of 500 ml min^{-1} at STP fed at 2.5 bar(abs) pressure.

The peak power output of the DFAFC with PdSn/C and 1.27 g L^{-1} Nafion® was about 220 W m^{-2} at 333 K, while the power density of 80 W m^{-2} was associated with no Nafion® content. Thus, three times enhancement of the maximum power was achieved by incorporating the Nafion® content of 1.27 g L^{-1} in the anode structure (Figure 5-14). It is believed that a high Nafion® content would block the electrode pores and increases both the mass transfer and Ohmic resistance in the case of high Nafion® aggregates concentration within the catalyst layer (Kanga et al, 2010).
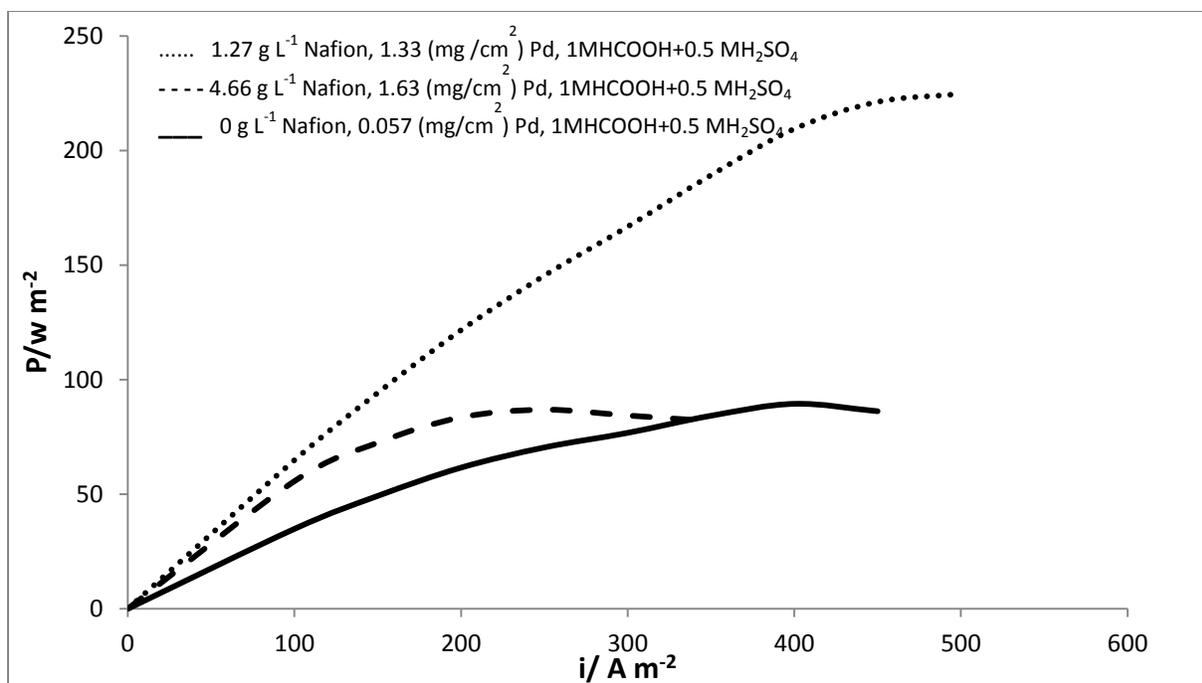
Figure 5-14: Power density of DFAFC at 333 K .Fuel feed: 1 M HCOOH with 0.5 MH$_2$SO$_4$ at 3 mL min^{-1}; Cathode feed: dry O$_2$ fed at 2.5 bar(abs) and flow rate of 500 mL min^{-1}at STP.
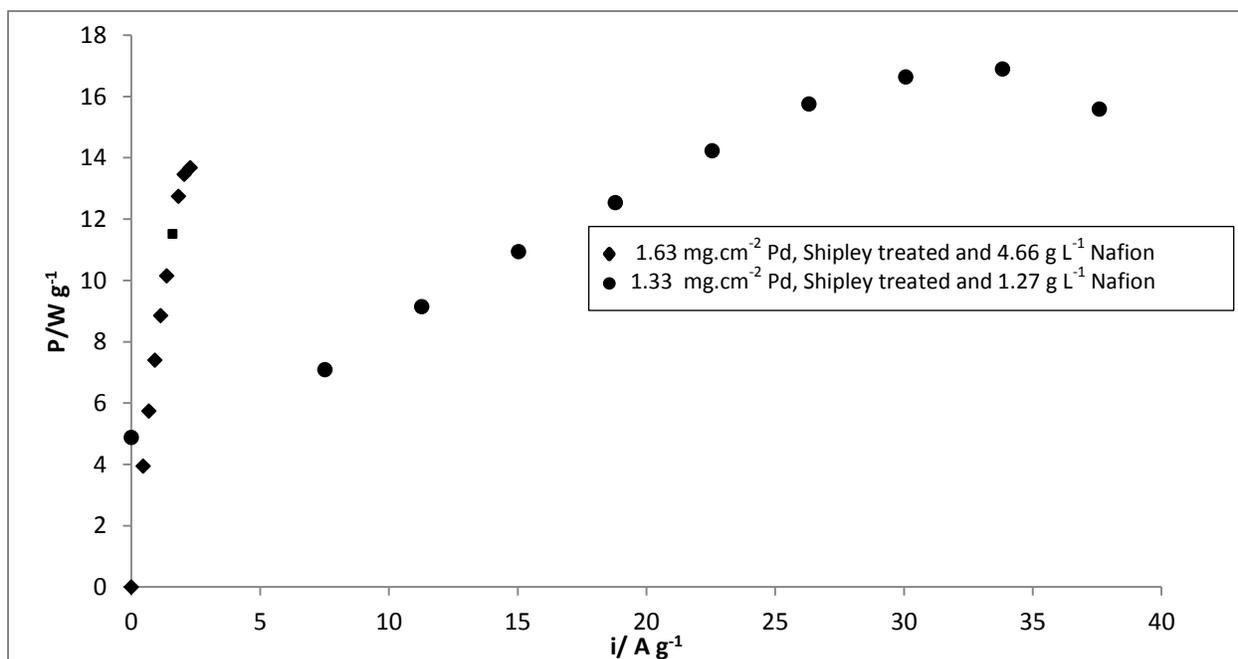
Figure 5-15:DFAFC performance at 333 K based on anode catalyst mass basis- effect of Shipley pre-treatment .The Pd/C was prepared with 1.27 g L^{-1}and 4.66 g L^{-1} Nafion® . Fuel feed: 1 M HCOOH with 0.5 M H$_2$SO$_4$ and 3 ml min^{-1}; Cathode feed: dry O$_2$ fed at 2.5 bar(abs) and flow rate of 500 mL min^{-1} at STP.

5.2.1 DFAFC Polarization experiments on anode activated in 5 wt% nitric acid

The performance comparison of carbon fiber supported Pd, pre-treated in 5 wt% nitric acid and untreated Pd/C is shown in Figure 5-16. Upon applying the nitric acid solution to activate the surface of carbon fiber, the electroless deposition yielded a Pd mass loading of 4.5 mg cm^{-2}. It is observed that the Pd/C pre-treated by nitric acid solution resulted in higher OCV of 0.77 V in DFAFC tests; while, with no nitric acid pre-treatment the OCV of 0.69 V is achieved. Both anodes were incorporated with 1.27 g L^{-1} in Nafion® solution (Figure 5-16).
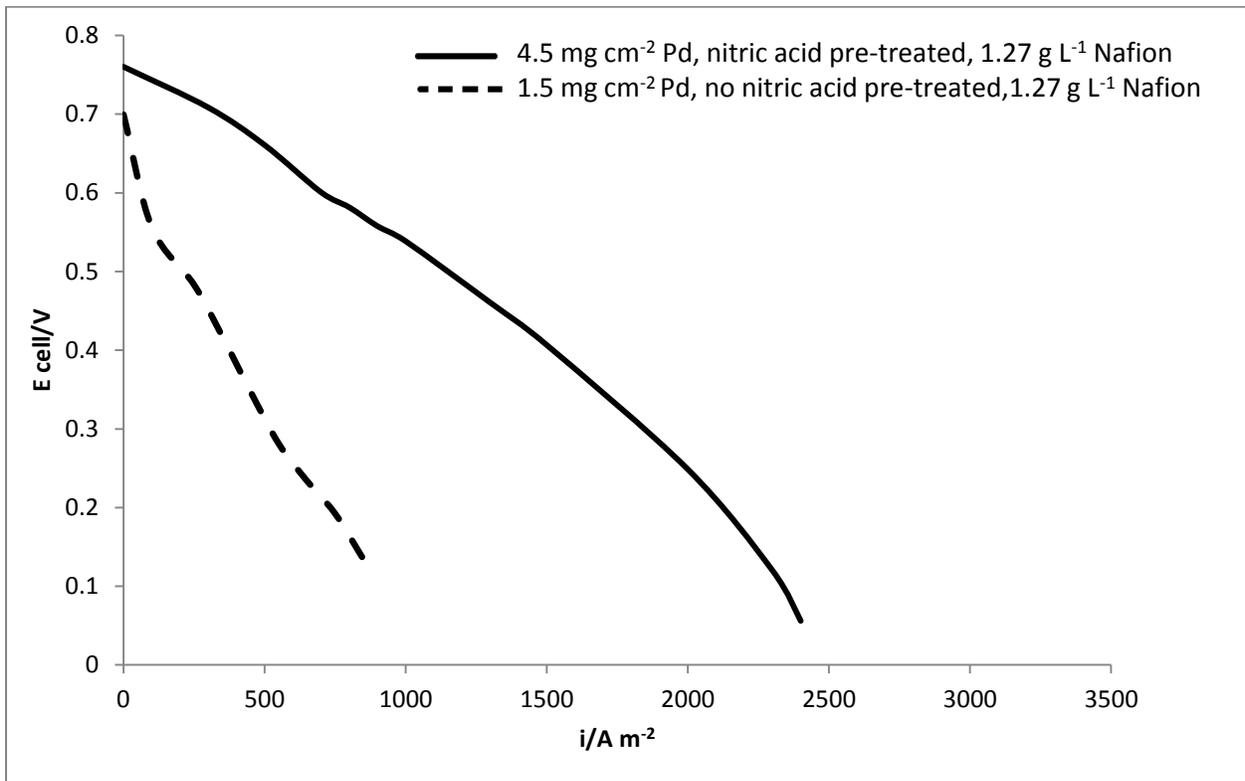
Figure 5-16: DFAFC polarization curve at 333 K-effect of 5 wt% nitric acid pre-treatment and 1.27 g L^{-1}Nafion® solution content. Fuel feed: 1 M HCOOH with 0.5 M H$_2$SO$_4$ at 3 ml min^{-1}; Cathode feed: dry O$_2$ fed at 2.5 bar(abs) and O$_2$ flow rate of 500 mL min^{-1} at STP.
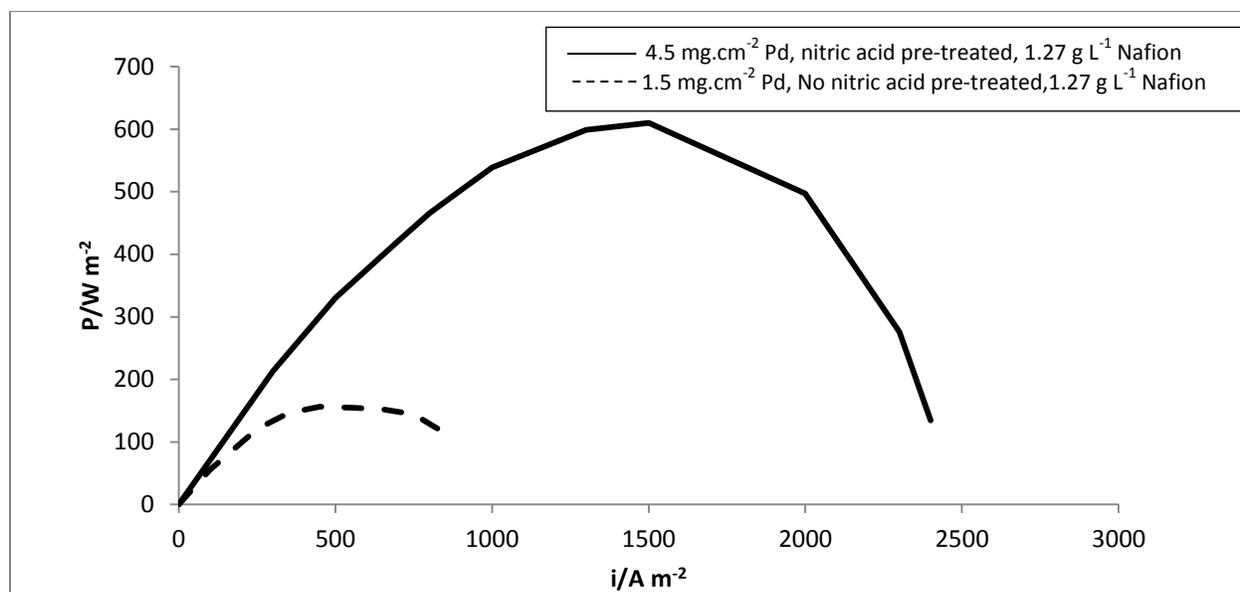
Figure 5-17:DFAFC power density curve at 333 K-effect of nitric acid pre-treatment .The Pd/C was prepared with 1.27 g L^{-1} Nafion® and 15 min treatment in 5 wt% nitric acid solution. Anode feed: 1 M HCOOH with 0.5 MH$_2$SO$_4$; Cathode feed: dry O$_2$ fed at 2.5 bar(abs) pressure and O$_2$ 500 mL min^{-1} flow rate at STP.

5.2.2   Long-term stability DFAFC tests

The stability and deactivation characteristics of anode electrodes were tested by drawing a constant current density of 100 A m^{-2} over a period of 5 hours (Figure 5-18). The results indicate that the performance of the two catalyzed carbon fibre electrodes affected by 1.27 g L^{-1} Nafion® content were fairly similar within 20 to 140 min time frame.

Comparing the Pd/C and PdSn/C performances in Figure 5-18, the Pd/C anode with higher Pd mass load (4.5 mg cm^{-2}) and operating cell voltage stays fairly stable on ~ 0.55 V up to 3.5 hours of constant current draw. However, the different pre-treatment methods employed in the activation of carbon substrates can also affects the stability of synthesised anode over time.

In the case of Shipley pre-treatment method, the existence of Sn(II) on the carbon fiber surface lowered the CO poising affect up to 3 hours of operation at 0.65 V. In a study done by Haan et al. the PdSn/C anode demonstrated better performance compared to Pd/C over 3 hours of cell operation (constant current drawn of 100 A m^{-2} at 323 K) . It is shown that PdSn/C anode demonstrated stronger resistance to CO build up compared to Pd/C (Haan & Masel, 2009).

However, an overall superior performance of Pd/C anode can be explained by 3 times higher loading compared to PdSn/C. After 5 hours, Pd/C anode performance decreased to half of the initial voltage and followed a sharp voltage drop soon after.

On the other hand, the OCV corresponding to the catalyzed anode with no Nafion® content (low Pd mass loading of 0.057 mg cm^{-2}) is very low and the cell voltage dropped quickly after 10 min of continuous operation.
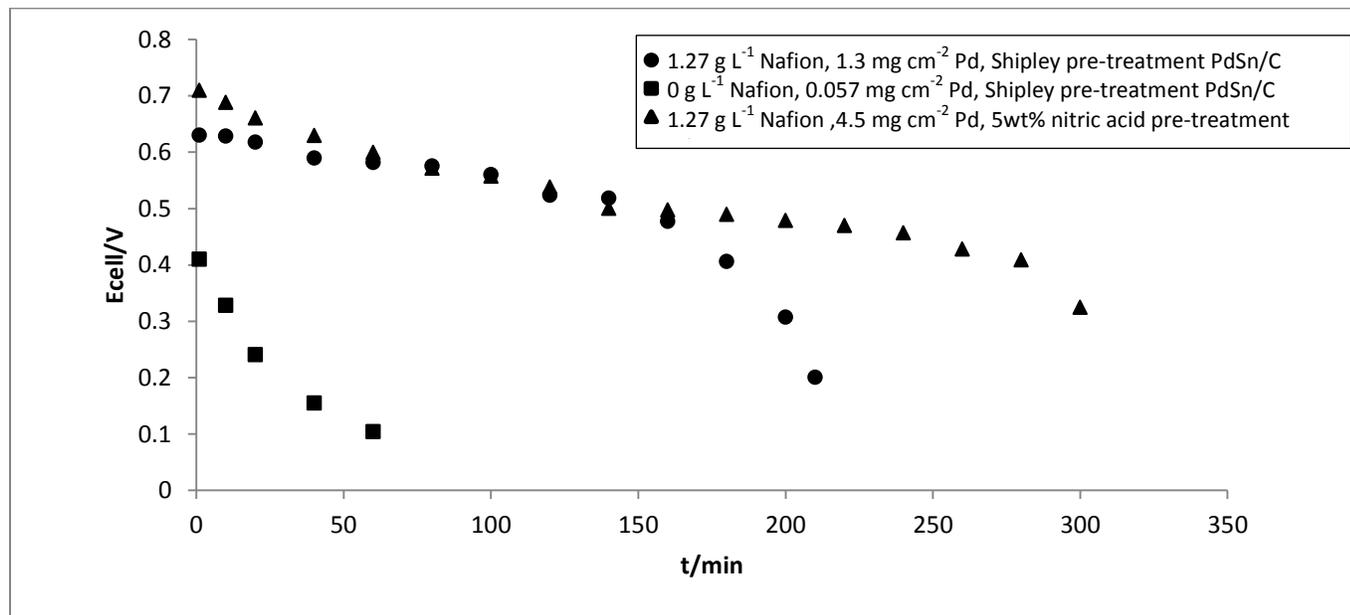
Figure 5-18: Constant current (100 A m^{-2}) experiments for three different Pd-based anode catalysts in the direct formic acid fuel cell at 333 K. Anode feed: 1 M HCOOH with 0.5 M H$_2$SO$_4$, flow rate of 3 cm^3 min^{-1}; Cathode feed: dry O$_2$ fed at 2.5 bare(abs) pressure and O$_2$ flow rate of 500 mL min^{-1}at STP.

Zhu and co-workers studied the behaviour of DFAFC Pd-based anode under constant-current operation (Zhua, Khan, & Masel, 2005). According to their study the highest CO$_2$ generation occurs at the surface that is free of (COOH)$_{ads}$ for the electrodes with catalyst particles size of around ~6 nm (explained in Equation 5-1 through 5-3). The presence of catalyst particle size of around 0.40 μm in this study is much larger than what Zhu and co-workers determined for free COOH$_{ads}$ sites and therefore poisoning by adsorbed COOH species may have contributed to the present observed deactivation.

$$HCOOH_{bulk} \rightarrow CO_2 + 2H^+ + 2e^- \qquad \text{[Eq. 5-1]}$$

$$HCOOH_{ad} \rightarrow (COOH)_{ads} + H^+ + e^- \qquad \text{[Eq. 5-2]}$$

$$(COOH)_{ads} \rightarrow CO_2 + H^+ + e^- \qquad \text{[Eq. 5-3]}$$
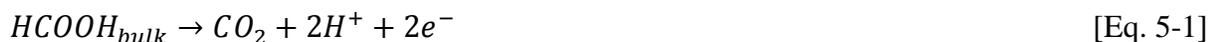
Although the oxidation of formic acid in this study is suggested to occur through the non-CO pathway at Pd surface, the presence of weakly adsorbed poisoning species such as COOH$_{ads}$ lowers the oxidation reaction rate and hence increase the anode overpotential over time.

Higher concentration of formic acid fuel would facilitate the FC system design and is desirable for use in portable power application. Therefore, a series of fuel cell tests were performed to analyze the catalytic activity at 10 M formic acid in comparison with 1 M HCOOH. Polarization curve obtained (Figure 5-19) indicates notable higher OCV for 4.66 g L^{-1} Nafion® assisted electrode.

It is generally accepted that an increase in direct liquid fuel concentration would increases the fuel crossover that lowers the cell performance, and cause cathode flooding. Also, the impurities that are commonly found in commercial formic acid such as acetic acid and methyl formate might existe in higher concentration that could negatively affect the performance of Pd anodes when using 10 M formic acid (Pickup & Yu, 2009).

The high concentration of formic acid increases the aggregation and interaction between molecules in the concentrated solution such that it reacts differently to temperature and experimental conditions than the dilute solution. Therefore a more complex form of formic acid that arises at higher concentrations could kinetically be less active than dilute solution (Kang et al, 2010).
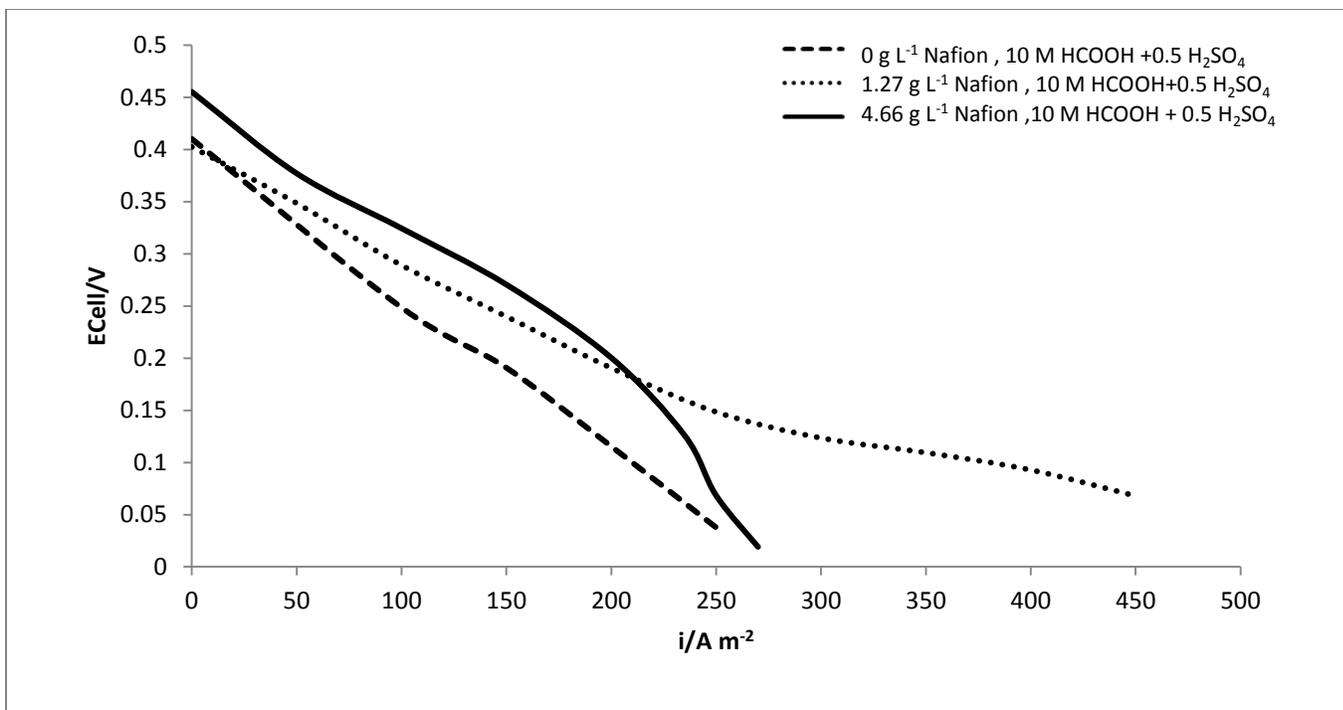
Figure 5-19: DFAFC polarization curve at 333 K- effect of 10 M HCOOH. Fuel feed: 10 M HCOOH, 0.5 M H$_2$SO$_4$, flow rate of 3 cm^3 min^{-1}; Cathode feed: dry O$_2$ fed at 2.5 bar(abs)pressure and O$_2$ flow rate of 500 mL min^{-1} at STP.

6.0   Conclusion

Palladium and PdSn particles supported on AvCarb ^{TM} P50 have been prepared by electroless deposition technique. To enhance the mass loading of catalyst on the carbon fiber support (AvCarb ^{TM} P50) two sensitization methods of acid wash (5 wt% HNO_3 solution) and Sn/Pd (Shipley-type solution) were applied.

Pre-treatment of the AvCarb^{TM} P50 in 5 wt% nitric acid solution followed by employing 1.27 g L^{-1} Nafion® as an additive in the electroless solution was essential to improve the surface adherence characteritics and wettability of AvCarb^{TM} P50 that promoted formic acid oxidation and more uniform catalyst dispersion. Dispersion of Pd particles (~0.45μm) throughout the thickness of substrate was achieved with maximum mass loading of 4.5 mg cm^{-2}. The successful surface activation of AvCarb^{TM} P50 with 5 wt% nitric acid solution could be explained by the presence of chemical functional groups (mainly surface oxides) that roughen the surface and improves the catalytic activity towards Pd ion reduction in the electroless bath.

To understand the impact of Nafion® solution (5 wt% ionomer solution) on the electroless deposition process (at 323 K), three different concentrations of pure Nafion® (1.27, 2.46 and 4.66 g L^{-1}) were studied . The Nafion® concentration in solution had a major impact on the catalyst dispersion and the resulting mass load . The subtrates pre-treated in 5 wt% nitric acid solutions showed 7 fold increase of Pd mass loading (from 0.60 mg cm^{-2} to 4.5+/- 0.1 mg cm^{-2}) when then concentration of Nafion® in solution increased from 0 to 1.27 g L^{-1}. It was demonstrated the longer exposure of substrate to chemical bath within 20 min to 45 min enhanced the dispersion of Pd particles in terms of increased mass loading.

In addition to acid nitric pre-treatment, the effect of pre-treatment with Shipley-type solution (6 mM PdC1$_2$ and 0.3 M SnC1$_2$ in 4 M HCL) on the surface activation was investigated. Treating the AvCarb^{TM} P50 with Shipley-type solution led to a more uniform deposit and smoother Pd coverage compared to nitric acid pre-treated substrate.

Comparing two different treatment times of 30 min and 60 min with Shipley solution, it was observed the longer pre-treatment time at constant temperature of 323 K led to lower intrinsic catalytic activity and negatively affected the surface morphology of the substrate by blocking the active surface sites (at Nafion content of 4.66 g L^{-1}). However, the presence of SnO_2 and Sn(II) species is believed to promote the catalytic activity and the overall DFAFC performance. Compared to un-treated carbon fiber, the substrate pre-treated in Shipley solution

for 30 min resulted in a fairly dense coating with Pd agglomerates of diameter ranging from 0.50-0.55 µm.

DFAFC operation at 100 A m^{-2} using (1 M HCOOH and 0.5 M H$_2$SO$_4$) for a period of 3.5 hours was fairly stable and may be explained by the effective contact between Pd catalyst particles and Nafion® ionomer which leads to better catalyst layer utilization.

The stability characteristics of Pd/C and PdSn/C pre-treated with nitric acid and Shipley solution were fairly similar. After 5 hours of continuous operation the Pd/C samples deactivated at the current density of 100 A m^{-2} at 333 K and 42% voltage drop.

In conclusion, a simple and cost-effective procedure for the synthesis of uniform Pd catalyst layer on carbon fiber anode material is developed. The effects of treatment time and Nafion® concentration on Pd particle size and catalytic activity were examined to determine the best experimental conditions. The approach of utilizing three-dimensional carbon fiber for anode design in electroless deposition method was shown to be an easy to follow method that successfully improved the catalyst morphology towards better activity and stability.

7.0   Recommendation and future work

- It is recommended to investigate the effect of higher Sn mass loading in binary PdSn/C substrates to understand the sole effect of Sn metal in DFAFC life test and polarization tests .

- The performance of 3-D anode must be thoroughly compared against CCM and GDE substrates.

- It is clear that the Pd catalyst becomes poisoned and periodic regeneration is required in order to investigate the commercial use of this anode catalyst in any practical DFAFC. Therefore, it is recommended to determine the conditions required to regenerate the Pd catalyst.

- It is recommended to measure the electrochemically active Pd surface area using the Cu underpotential technique (UPD).

References

Acosta, D., & Garcia, L. (2010, January 15). Development of Pd and Pd–Co catalysts supported on multi-walled carbon nanotubes for formic acid oxidation. *Journal of Power Sources, 195*(2), pp. 461-465.

Allen, R. G., Chan, L., Yang, L. X., Scott, K., & Roy, S. (2005). Novel anode structure for the direct methanol fuel cell. *Journal of Power Sources, 143*, pp. 142–149.

Arenz, M., Stamenkovic, V., & Schmidt, T. J. (2003). The electro-oxidation of formic acid on Pt–Pd single crystal bimetallic surfaces. *Physical Chemistry Chemical Physics, 5*, pp.4242-4251.

Argyropoulos, P., Scott, K., & Tamma, W. (1999). Carbon Dioxide Evolution Patterns in DirectMethanol Fuel Cells. *Electrochimica Acta, 44*(20).

Barbir, F. (2005). Pem Fuel Cells: Theory and Practice (Vol. 465). Elsevier Inc.

Bard, A., & Faulkner, L. (2001). *Electrochemical Methods, Fundamentals and Applications*. New York: Wiley & Sons.

Bauer, A., Gyenge, E. L., & Oloman, C. W. (2007, May 15). Direct methanol fuel cell with extended reaction zone anode: PtRu and PtRuMo supported on Graphite Felt. *Journal of Power Sources, 167*(2), pp. 281–287.

Bauer, A., Gyenge, E., & Oloman, C. W. (2006, July 28). Electrodeposition of Pt–Ru nanoparticles on fibrous carbon substrates in the presence of nonionic surfactant: Application for methanol oxidation. *Electrochemica Acta, 51*(25), pp. 5356–5364.

Bauer, A., Lee, K., & Song, C. (2010, May 15). Pt nanoparticles deposited on TiO2 based nanofibers: Electrochemical stability and oxygen reduction activity. *Journal of Power source, 195*(10), pp. 3105-3110.

Bauer, A., Oloman, C. W., & Gyenge, E. L. (2009, September 5). Three-dimensional anode engineering for the direct methanol fuel cell. *Journal of Power Sources, 193*(2), pp. 754–760.

Blair, S., & Lycke, D. (2006, November 3). Palladium-Platinum Alloy Anode Catalysts for Direct Formic Acid Fuels. *Electrochemical Society, 13*(1), pp. 1325-1332.

Blomen, L. J., & Mugerwa, M. N. (1993). *Fuel Cell Systems*. New York : Plenum Press.

Campanati, M., & Fornasari, G. (2003, January 15). Fundamentals in the preparation of heterogeneous catalysts. *Catalysis Today, 77*(4), pp. 299-314.

Capon, A., & Parsons, R. (1973, May 25). The oxidation of formic acid at nobel metal electrodes. *Journal of Electroanalytical Chemistry and Interfacial Electrochemistry, 44*(1), pp. 1-7.

Carrette, L., & Friedrich, A. K. (2000, December 15). Fuel cell types: Types, Fuel and Application. *Chemical physics and physical chemistry, 1*(163-192), pp. 162-193.

Chan, K., Yong, J. K., & Takashi , Y. (2004, August 16). High performance of cup-stacked-type carbon nanotubes as a Pt–Ru catalyst support for fuel cell applications. *Journal of applied physics, 96*, pp. 5903-5907.

Chen, Y., & Zhou, Y. (2010, July 1). Electrocatalytic properties of carbon-supported Pt-Ru catalysts with the high alloying degree for formic acid electrooxidation. *Journal of Power Sources, 195*(13), pp. 4129-4134 .

Chen, Y., Heinen, M., & Jusys, Z. (2005). Kinetics and Mechanism of the Electrooxidation. *Journal of Electrocatalysis, 45*, pp. 981-985.

Cheng, T. T., & Gyenge, E. L. (2006, May 20). Electrodeposition of mesoscopic Pt-Ru on reticulated vitreous carbon from reverse emulsions and from reverse emulsions and microemulsions: Application to methanol electro-oxidation. *Electrochimica Acta, 51*(19), pp. 3904–3913.

Cheng, T. T., & Gyenge, E. L. (2008, June 13). Efficient Anodes for Direct Methanol and Formic Acid Fuel Cells:the Synergy Between Catalyst and Three-Dimensional Support. *Journal of Electrochemical Society, 155*(8), pp. B819-B828.

Cheng, T. T., & Gyenge, E. L. (2009, November 10). Novel catalyst-support interaction for direct formic acid fuel cell anodes: Pd electrodeposition on surface-modified graphite felt. *Journal of Applied Electrochemistry, 39,* pp. 1925-1938.

Cohen, R., & Mekk, R. (1976, April 1976). The Chemistry of Palladium-Tin Colloid Sensitizing Processes. *Journal of Colloid and Interface Science, 55*(1), pp. 156-162.

Duck Han, S., & Choi, J. (2009). Performance characterization of direct formic acid fuel cell. *Korean Journal of Chemical Engineering, 26*, pp. 1040-1046.

Glenn, O., Mallory , B., & Juan, H. (1990). *Electroless Plating fundamentals & applications*. New York: William Andrew Publishing .

Haan, J., & Masel, R. (2009). The influence of solution pH on rates of an electrocatalytic reaction: Formic acid electrooxidation on platinum and palladium. *Electrochimica Acta, 54*, pp. 4073-4078.

Horkans, J. (1983). A Cyclic Voltammetric Study of Pd-Sn Colloidal Catalysts for Electroless Deposition. *Journal of Electrochem Soc,132*(22), 311-317.

J.H Choi, S. N. (2008). Formic acid oxidation by carbon-supported palladium catalysts in direct formic acid fuel cell. *Korean Journal of Chemical Engineering, 25,* pp. 1026-1030.

Jean, H. (2005). *A Cyclic Voltammetric Study of Pd-Sn Colloidal Catalysts for DFAFC*. New York: Thomas J. Watson Research Center.

Jeonga, K., Miesse, C., & Cho, J. (2007, May 25). Fuel crossover in direct formic acid fuel cells. *Journal of Power Sources, 168*(1), pp. 119-125.

Kang, S., Lee, J. K., & Chung, S. Y. (2006). Influence of Bi Modification of Pt Anode Catalyst in Direct Formic Acid Fuel Cells. *Journal of Physical Chemistry, 110*, pp. 7270-7274.

Kanga, Y., Mingjun, R., & Ting, Y. (2010, May 1). Effect of Nafion aggregation in the anode catalytic layer on the performance of a direct formic acid fuel cell. *Journal of Power Sources, 195*(9), pp. 2649–2652.

Kinoshita, K. (1988). *Carbon: Electrochemical and Physicochemical Properties*. Berkeley ,California: John Wiley and Sons Inc.

Kojima , K., & Hideto, W. (2010, August 12). *Patent No. 20100199882.*

Koper, M. (2009). *Fuel Cell Catalyst*. New Jersey: John Wiley & Sons, Inc.

Langer, S., & Tri, D. T. (1993, August 21). Graphite pre-treatment for deposition of platinum catalysts. *Electrochemica Acta, 38*(11), pp. 1551-1554.

Larsen, R., Zakzeski, J., & Masel, R. I. (2006, June 19). Unusually active palladium-based catalysts for the direct formic acid fuel cell. *Journal of Power Sources, 157*, pp. 78-84.

Li, j., Lei, M., & Xianian, L. (2005, June 3). Effect of nitric acid pre-treatment on the properties of activated carbon and supported palladium catalysts. *Ind. Eng. Chem. Res, 44*, pp. 5478-5482.

Li, X., & Hsing, M. (2006, April 25). Electrooxidation of formic acid on carbon supported Pt-Pd nanocatalysts. *Electrochimica Acta, 51*, pp. 3477–3483.

Lister, S., & McLean, G. (2004). PEM fuel cell electrodes. *Journal of Power Sources, 130*, pp. 61-76.

Liu, Z., & Liang, H. (2006, July 27). Nanostructured Pt/C and Pd/C catalysts for direct formic acid fuel cells. *Journal of Power Sources, 161*(2), pp. 831-835.

Liu, Z., & Xinhu, Z. (2009, August). Carbon-supported PdSn nanoparticles as catalysts for formic acid oxidation. *Electrochemistry Communications, 11*(8), pp. 1667–1670.

Markovic, N. M., & Gasteiger , H. A. (1995). Electro oxidation mechanism of formic acid of Pt-Ru alloy surfaces. *Electrochemica Acta, 40*, pp. 91-98.

Mathur, V., & Crawford, J. (2000). *Fundamentals of Gas Diffusion Layers in PEM Fuel Cells*. New Delhi, India: John Wiley and Sons.

Mauritz, K. A., & Moore, B. R. (2004, July 19). State of understanding of Nafion. *Chem. Rev, 104*, pp. 4535-4585.

McGoverna, M., Garentta, E., & Rice, C. (2003). Effects of Nafion as a binding agent for unsupported nanoparticle catalysts. *Journal of Power Sources, 114*, pp. 35-39.

McNicol , B., Rand b, D., & Williams, K. (1999, October). Direct methanol–air fuel cells for road transportation. *Journal of Power Sources, 83*(15), pp. 15-31.

Miley, G. H., Luo, N., & Mather, J. (2007, March 20). Direct NaBH4/H2O2 fuel cells. *Journal of Power Sources, 165*(2), pp. 509-516.

Montes-Moan, M., & suarez, D. (2004, February 8). On the nature of basic sites on carbon surfaces: An overview. *Carbon, 42*(7), pp. 1219–1225.

Niquirilo, R., & Teixeira-Neto, E. (2010, March 31). Formic acid oxidation at Pd, Pt and PbOx-based catalysts and calculation of their approximate electrochemical active areas. *Journal of Electrochemical, 5*, pp. 344-354.

Okamoto, H., Kon, W., & Mukouyama, Y. (2005, July 27). Five current peaks in voltammograms for oxidations of formic acid, formaldehyde, and methanol on platinum. *Journal of Physical Chemistry, 109*(32), pp. 15659-15666.

Pan, Y., & Zhang, R. (2009, December 23). Anode poisoning study in direct formic acid fuel cells. *Electrochemical and Solid-State, 12*(3), pp. B23-B26.

Passalacqua, E., & Lufrano, F. (2001, January 1). Nafion content in the catalyst layer of polymer electrolyte fuel cells: effects on structure and performance. *Electrochimica Acta, 46*(6), pp. 799–805.

Pickup, P. G., & Yu, X. (2009, November 13). Deactivation/reactivation of a Pd/C catalyst in a direct formic acid fuel cell. *Journal of Power Sources, 187*, pp. 493–499.

R.S. Jayashree, J. S. (2005, August 30). Characterization and application of electrodeposited Pt, Pt/Pd, and Pd catalyst structures for direct formic acid micro fuel cells. *Electrochimica Acta, 50*(24), pp. 4674–4682.

Rhee, Y., Ha, S., & Masel, R. (2005). Crossover of formic acid through Nafion membranes. *Journal of Power Sources, 117*, pp. 11735-11738.

Rice, C., & Masel, R. (2003, April 10). Catalysts for direct formic acid fuel cells. *Journal of Power Sources, 115*(2), pp. 229-235.

Rice, C., & Masel, R. I. (2003). Catalysts for direct formic acid fuel cells. *Journal of Power Sources, 115*, pp. 229–235.

Rice, C., Haa, S., & Masel, R. (2002, April 25). Direct formic acid fuel cells. *Journal of Power Sources, 111*, pp. 82-89.

Ristinen, A. R., & Kraushaar, J. P. (2006). *Energy and the Environment*. John Wiley & Sons. Inc.

S. Song, G. W. (2005, January 10). The effect of the MEA preparation procedure on both ethanol crossover and DEFC performance. *Journal of Power Sources, 140*(1), pp. 103-110 .

Shao, Z. G., Zhu, F., Lin, W. F., & Christensena, P. A. (2006). PtRu/Ti anodes with varying Pt :Ru ratio prepared by electrodeposition for the direct methanol fuel cell. *Phys. Chem. Chem. Phys., 8*, pp. 2720-2726.

Shen, W., Li, Z., & Liu, Y. (2008, November 2). Surface Chemical Functional Groups Modification of Porous Carbon. *Chemical Engineering, 1*, pp. 27-40.

Shu, J., & Grandjean, P. A. (1993, November 5). Autocatalytic effects in electroless palladium deposition. *Journal of Electrochemical Society, 140*(11), pp. 3175-3180.

Song, S. Q., & Zhou, W. J. (2004). Direct methanol fuel cells: methanol crossover and its influence on single DMFC performance. *Journal of Fuel Cell Science and Technology, 10*, pp. 458-462.

Stafford, K. M., Richard, I., & Haan, J. L. (2010, June 14). Effects of the addition of antimony, tin, and lead to palladium catalyst formulations for in DFAFC. *Journal of Physical. Chemistry, 114*(26), pp. 11665–11672.

Su-Jen Lee, T. L. (2004, April). Solution properties of nafion in methanol/water mixture solvent. *Polymer, 45*(8), pp. 2853–2862.

Sun, L., Ran, R., & Wang, G. (2008). Fabrication and performance test of a catalyst-coated membrane from direct spray deposition. *Solid State Ionics, 179*, pp. 960-965.

T. Shuihua, S. (2010). Review of new carbon materials as catalyst supports in direct alcohol fuel cells. Chinese *Journal of Catalyst, 31*(1), pp. 12-17.

Tester, J., Drake, E., & Golay, M. W. (2005). *Sustainable energy: choosing among options*. London: Massachusetts Institute of Technology .

Tran, T. D., & Langer, S. H. (1993). Graphite pre-treatment for deposition of Pt Catalyst. *Electrochimica Acta, 11*(38), pp. 1551-1554.

Uhm, S., Kwon, Y., & Chung, S. (2008, June 30). Highly effective anode structure in a direct formic acid fuel cell. *Electrochimica Acta, 53*(16), pp. 5162–5168.

Uhm, S., Lee, J., & Chung, S. (2008). Effect of anode diffusion media on direct formic acid fuel cells. *Journal of Industrial and Engineering Chemistry, 14*(2), pp. 493–498.

Venugopalan, S. (2001). *Micro Fuel Cells*. New Delhi, India: Anamaya Publishers.

Volpe, M., Inguanta, R., Piazza, S., & Sunseri, C. (2006, May 22). Optimized bath for electroless deposition of palladium on amorphous alumina membranes. *Surface & Coatings Technology, 200*(20), pp. 5800–5806.

Wang, J. (2006). *Analytical Electrochemistry*. New Jersey: John Wiley and Sons.

Wang, Z., & Geping, Y. (2007). Preparation and influence of performance of anodic catalysts for direct methanol fuel cell. *Frontiers of Chemical Engineering in China, 1*(1), pp. 20-25.

Weber, M., & Wang, J. (1996, July 10). Formic acid oxidation in a polymer electrolyte fuel cell. *Journal of Electrochemical Society, 43*(7), pp. L158-L160 .

Weijiang Zhou, Z., & Lee, J. (2007). Highly active core–shell Au/Pd catalyst for formic acid oxdiation. *Electrochemistry Communications, 9*, pp. 1725–1729.

Wu, Z., U, C., & Pittman, J. (1995, March 17). Nitric acid oxidation of carbon fibers and the effects of subsequent treatment in refluxing aqueous NaOH. *Carbon, 33*(5), pp. 597-605.

Xiaoming , R., & Henderson, W. (1997, June 2). Electro-osmotic drag of water in ionomeric membranes. *Journal of Electrochemical Society, 144*, pp. L267-L271.

Yu, X., & Pickup, P. (2008, July 15). Recent advances in direct formic acid fuel cells (DFAFC). *Journal of Power Sources, 182*(1), pp. 124-132.

Zhu, Y., & Masel, R. (2004, November 25). High power density direct formic acid fuel cells. *Journal of Power Sources, 130*, pp. 8-14.

Zhu, Y., Uchida, H., & Watanabe, M. (1999). Oxidation of carbon monoxide at a platinum film. *Langmuir, 15*(25), pp. 8757-8764.

Zhua, Y., Khan, Z., & Masel, R. I. (2005, August 28). The behavior of palladium catalysts in direct formic acid fuel cells. *Journal of Power Sources, 139*(2), pp. 15-20.

Appendix A- nafion® mass concentration sample calculation

Adding 1.5 ml of Nafion® (5 wt% solution) in 50 ml of electroless bath corresponds to 1.27 g/L pure Nafion® as calculated below:

Density of Nafion® (5 wt% solution) = 0.87 g ml^{-1}

$$\text{Nafion content} \left(\frac{\text{g}}{\text{mL}}\right) = \frac{\left[1.5 \text{ ml Nafion} \times 0.87 \frac{g}{ml} \times 0.05 \frac{g}{g}\right]}{[50 \ ml \ electroless \ solution + 1.5 \ ml \ Nafion \ ]} = 0.00127 \ \frac{g}{L}$$

[Eq. A-1]

Conversion to g/L:

$$0.00127 \ \frac{g}{mL} pure \ Nafion \ \times 1000 = 1.27 \ \frac{g}{L}$$